NASA TECHNICAL MEMORANDUM

NASA TM X-1671

NASA TM X-1671

STUDIES OF FLOW DISTORTION IN THE TAILPIPES OF HYDROGEN PEROXIDE GAS GENERATORS USED FOR JET-ENGINE SIMULATION

by Leland B. Salters, Jr., and Nicholas C. Chamales

Langley Research Center

Langley Station, Hampton, Va.

NATIONAL AERONAUTICS AND SPACE ADMINISTRATION • WASHINGTON, D. C. • OCTOBER 1968

NASA TM X-1671

STUDIES OF FLOW DISTORTION IN THE TAILPIPES OF HYDROGEN PEROXIDE GAS GENERATORS USED FOR JET-ENGINE SIMULATION

By Leland B. Salters, Jr., and Nicholas C. Chamales

Langley Research Center
Langley Station, Hampton, Va.

NATIONAL AERONAUTICS AND SPACE ADMINISTRATION

For sale by the Clearinghouse for Federal Scientific and Technical Information
Springfield, Virginia 22151 – CFSTI price $3.00

STUDIES OF FLOW DISTORTION IN THE TAILPIPES OF HYDROGEN PEROXIDE GAS GENERATORS USED FOR JET-ENGINE SIMULATION

By Leland B. Salters, Jr., and Nicholas C. Chamales
Langley Research Center

SUMMARY

An investigation has been made of the effect of variation in configuration of hydrogen peroxide decomposition engines on the jet-exhaust-flow characteristics. Sixteen configurations of hydrogen peroxide decomposition engines were tested under static conditions over a jet-exit total-pressure to static-pressure ratio range from 1.2 to 4.6 using hydrogen peroxide of approximately 90.5-percent concentration. Jet-exit total-pressure flow distortion was found to vary inversely with the contraction ratio of the tailpipe. The propellant-distribution-plate and catalyst-bed retainer-plate designs also influenced exhaust-flow patterns. Flow-straightener plates were effective in reducing flow distortion in the jet exhaust.

INTRODUCTION

A method for simulating jet-engine exhaust by means of the hydrogen peroxide gas generator has been developed at the Langley 16-foot transonic tunnel for wind-tunnel models as described in reference 1. The effectiveness of this method, particularly in nozzle-performance studies, depends to a large extent on the accurate measurement of the total pressure in the jet-exhaust stream.

Currently, total pressure is measured by means of a single probe, or at most two probes, located in the tailpipe, one to two nozzle diameters upstream of the jet exit. In order to obtain an accurate average value for the total pressure across the stream with only one or two probes, the total-pressure distribution across the stream must be uniform. Furthermore, uniform flow distribution is desirable for accurate simulation of jet-interference effects.

Some of the gas generator and tailpipe configurations used at the Langley 16-foot transonic tunnel have produced nonuniform flows in the jet streams, the degree of distortion varying with the configuration.

The method used in current practice to correct for the effect of flow distortion on the probe readings is calibration of the engines under static conditions prior to wind-tunnel tests. Total pressures are measured simultaneously by the probes and by a rake located in the jet-exit plane. By comparing the pressures obtained by the two different methods, a factor is obtained for correcting the probe readings as recorded during wind-tunnel tests.

In order to pinpoint the sources of the distortion and to evaluate methods of straightening the flow, a study was made of the effect of the engine geometry and total-pressure distributions in the jet exits for 16 engine simulators used in the models tested in the Langley 16-foot transonic tunnel.

SYMBOLS

A_j cold area of jet nozzle throat, centimeters^2 (inches^2)

A_j' nozzle-throat area after thermal expansion, centimeters^2 (inches^2)

A_{max} maximum internal cross-sectional area of tailpipe, centimeters^2 (inches^2)

H_2O_2 hydrogen peroxide

M Mach number

N_2 nitrogen

p_a barometric pressure, newtons/centimeter^2 (pounds/inch^2 absolute)

$p_{t,j}$ jet total pressure measured by probes inside engine tailpipe, newtons/centimeter^2 (pounds/inch^2 absolute)

$p_{t,max}$ maximum total pressure in jet-exit plane, newtons/centimeter^2 (pounds/inch^2 absolute)

$p_{t,min}$ minimum total pressure in jet-exit plane (within limits of $r/R = \pm 0.90$), newtons/centimeter^2 (pounds/inch^2 absolute)

$p_{t,r}$ area-weighted average jet total pressure measured by rake, newtons/centimeter^2 (pounds/inch^2 absolute)

r radial distance from jet center line, centimeters (inches)

R radius of nozzle throat, centimeters (inches)

γ flow-distortion factor, $\frac{p_{t,max} - p_{t,min}}{p_{t,r}} \times 100$, percent

γ_{av_3} average flow-distortion factor of three curves containing highest values of total-pressure ratio for each run, percent

APPARATUS

The hydrogen peroxide decomposition engines were tested under static conditions in the static-test facility of the Langley 16-foot transonic tunnel. The photographs of figures 1(a) and 1(b) present two views of engine configuration I mounted on the thrust balance in the test pit. Figure 1(c) is a sketch of the cruciform rake, pictured in figure 1(b), which was used to obtain static-pressure and total-temperature measurements. Figure 2 is a schematic diagram of the test apparatus. The nitrogen-feed pressure was controlled by means of the pressure-regulator valve, and the hydrogen peroxide flow rate was controlled by the flow-control valve. The shut-off valve was used to insure complete shut-off of the flow during periods of inactivity. The flow rate was measured by two rotating-vane flowmeters, and the thrust was measured by a strain-gage load cell mounted in a flexure-plate-supported platform. Pressures were measured by pressure transducers and temperatures were measured by thermocouples. The electrical outputs of the instruments were recorded on an oscillograph or on magnetic tapes.

The 16 engine-simulator configurations included in the investigation are sketched in figure 3, and photographs of typical distribution plates, retainer plate, and flow-straightener plate are presented in figure 4. The distribution plates of figures 4(a) and 4(b) contain holes of reduced size near the centers of the plates. The purpose in this arrangement is to prevent excessive H_2O_2 flow through the center of the plate. Excessive flow at the center produces excessive bed erosion in the center of the beds.

Typical catalyst-bed arrangements used in the 10.16-cm (4-in.) diameter and larger configurations are shown in the appendix and in the photograph of figure 5. Those of the 7.34-cm (2.89-in.) diameter configurations, used only in engine configurations IIIA to IIID, are also presented in the appendix. The antichannel baffles mentioned in the appendix are rings used to reduce the leakage of hydrogen peroxide around the edges of the beds. Each screen, in accordance with standard practice in packing beds, had its wire mesh oriented randomly to that of the other screens to prevent channeling of the

flow. The beds of both diameter sizes are essentially the same in composition. (See ref. 2 for the effect of bed composition on performance characteristics.)

Figure 6 is a sketch of configurations IA to IE. The open areas of the distribution plates for the engine configurations without flow-straightener plates, other than configuration IC, were on the order of 25 percent.

METHOD

The hydrogen peroxide decomposition engines were tested under static conditions over a range of pressure ratio $(p_{t,r}/p_a)$ from about 1.2 to 4.8. At the start of a typical test, the nitrogen pressure was set in the 653 to 798 N/cm^2 (450 to 550 psig) range by means of the pressure-regulator valve. The data for each point were taken after conditions became settled and points were taken in ascending and descending order over the pressure-ratio range.

Flow distortion was evaluated by means of the total-pressure distribution curves (figs. 7 and 8) and was arbitrarily defined as the maximum value of total pressure for each curve minus the minimum value (between the limits of ± 0.90 r/R) divided by the area-weighted average total pressure measured by the rake. The flow-distortion factor quoted for each engine was obtained from the average of the three curves containing the highest values of total-pressure ratio for each run.

Even though some low supersonic flow was observed in the jet exits, no corrections were made to the total-pressure data for its effect on the probes.

RESULTS AND DISCUSSION

Effect of Variation in Components

The effect on the flow-distortion factor of varying the components of the decomposition chamber and tailpipe of hydrogen peroxide decomposition engines is presented in figure 6 for a series of tests of configuration I. The largest distortion factor, namely 17.7 percent, was obtained with configuration IA. (See fig. 7(a).) The total-pressure distribution shows an extremely low valley in the center of the nozzle. Perhaps one reason for the decreased flow in the center was the bowing of the 0.635-cm-thick (0.250-in.) retainer plate during the tests. The bed was packed under considerable pressure, and during engine operation the retainer plate deformed under the effects of pressure and temperature. The bowing of the retainer plate tended to direct the flow towards the walls of the tailpipe and away from the center. This tendency was indicated by the fact that configuration IB, which contained the thicker (0.952-cm (0.375-in.))

retainer plate, produced a smoother flow pattern. (See fig. 7(b).) The thicker plate was not found to be bowed appreciably after the tests.

The effects on the flow-distortion factor of varying the open area of the distribution plates may be seen by comparing figure 7(b) (configuration IB) with figure 7(c) (configuration IC). Thus it may be seen that decreasing the open area from 25.6 percent to 5.2 percent had a smoothing effect on the total-pressure distribution.

The effect of the flow-straightener plates on the pressure-distribution patterns may be seen by comparing the curves for configurations ID (fig. 7(d)) and IE (fig. 7(e)) with configurations IB and IC. The addition of the flow-straightener plates improved the flow pattern in both instances, the beneficial effects being greater than those due to variation of either the distribution plates or the retainer plates. The fact that the flow-distortion factors of these two configurations (ID and IE) were nearly the same, although other components were not identical, indicates that the influence of the flow-straightener plates was great enough to mask the smaller influences due to the variation of other components.

The engines without the flow-straightener plate characteristically showed reduced total pressure in the center of the jet exits, whereas the engines using the flow-straightener plates showed increased total pressure in the center. The cause of the increased pressure in the center of the jet, as produced by flow-straightener plates, may be the restriction to the flow near the outer edges of the plates. As seen in the photograph of figure 4(d), blockage by the ring which is welded to the inner walls of the tailpipe and the reduction in the number of holes near the outer edges of the plate may have the effect of directing the flow away from the walls and toward the center of the tailpipe.

Repeatability of Data

Figure 8 presents the exit-plane total-pressure distributions for configurations II to IX. Several identical configurations were tested and included in this study to illustrate the repeatability or scatter of the data results. The results presented in figures 8(c) and 8(d) were obtained from different engines (configuration IIIB) that were constructed identically, according to the present state of the art. They had similar pressure-distribution patterns, in general, but the average flow-distortion factors were 8.0 percent and 8.9 percent for engines 1 and 2, respectively. Also, the results presented in figures 8(e) and 8(f) were obtained from different engines (configuration IIIC) constructed identically. For configuration IIIC, however, the pressure-distribution pattern for engine 1 was noticeably different from the pattern for engine 2 and the average flow-distortion factors were 10.3 percent and 6.1 percent for engines 1 and 2, respectively. Also included is a plot (fig. 8(g)) for configuration IIIC, engine 2, but with the initially used bed replaced by another. At the time the data of figure 8(g) were obtained, the

replacement bed had been operated for 2.55 hours and had deteriorated to the point that it was not completely decomposing the hydrogen peroxide. The results given in figure 8(g) are presented for comparison purposes only, since beds are normally replaced before they reach this stage of deterioration. (Incomplete decomposition of hydrogen peroxide is usually detected by a decrease in exhaust stagnation temperature.) The final pressure pattern was changed considerably from the original and the average flow-distortion factor increased from 6.1 percent to 10.9 percent.

The distortion parameter is a rough measure of flow distortion and is extremely sensitive to the minimum and maximum total pressure. This sensitivity accounts for the fact that there is some wide scatter in the data of identical configurations even though the shapes of the pressure distributions are very similar. To a lesser extent, some of the scatter in the data may have resulted from the fact that the rakes sampled pressures in only one plane through the jet. If measurements had been obtained in several planes and the average used, the results would probably have been more consistent.

Another small factor producing scatter in the data may have been the wakes of the total-pressure probes and thermocouples located in the tailpipes upstream of the rakes. The number and locations of the total-pressure probes and the location of the thermocouples varied between configurations so that there was no uniformity in the wake patterns. The rakes were positioned to minimize the effect of the wakes on the measurements.

For comparison, a typical pressure distribution for a full-scale turbojet airplane in flight is shown in figure 9. The data were obtained by means of a traversing probe installed in the jet stream of a fighter airplane equipped with afterburner and ejector-type nozzle (ref. 3). The total-pressure flow-distortion factor for the primary nozzle was 11 percent (arbitrarily computed within limits of the ±0.24-meter (±0.8-foot) radius since the traversing probe was some distance downstream of the primary nozzle exit).

Effect of Contraction Ratio

The distortion factors of figures 7 and 8 are presented in figure 10 as a function of contraction ratio $\left(A_{max}/A_j\right)$, which apparently exerted a great influence on the distortion factor. This figure indicates that for tailpipes with and without flow-straightener plates, in general, the distortion factor decreased with increase in contraction ratio. Unfortunately, due to space limitations in some wind-tunnel models, the maximum contraction ratio obtainable is somewhat less than desirable, so that some other means of obtaining uniform flow are required (such as using flow straighteners and modifying propellant-distribution plate and catalyst-bed retainer-plate designs). Figure 10 also indicates the improvement in pressure-distribution patterns produced by

flow straighteners. The scatter in the data, however, indicates that other factors such as the catalyst bed may influence the flow distortion.

Mach Number Distribution

In figure 11 is shown the static-pressure distribution along the internal surface of the tailpipe of configuration IB at a pressure ratio of 3.60. This distribution is compared with values computed from one-dimensional theory. The experimental Mach number distribution (computed from static- and total-pressure measurements) as compared with that for one-dimensional theory is also given. Reasonably good agreement is indicated between measured and theoretical values.

In order to study the Mach number distribution in and near the jet exit, static and total pressures and temperatures were measured at three axial locations: (1) in the plane of the jet exit, (2) upstream of the jet exit, and (3) downstream of the jet exit. The results are shown in figure 12. The lines are broken to indicate that the curves were made from a limited number of points. The data indicate that considerable variation in Mach number occurs in simple convergent nozzles across and in the plane of the jet exit for conditions of choked flow. In this particular instance (fig. 12(a)), the Mach number varied from about 0.7 at the center to over 1.1 near the nozzle lip. Mach numbers up to about 1.5 were calculated (from measured ratio of static pressure to total pressure) near the lips for some configurations tested.

The effect of total pressure on the sonic lines is shown in figure 12(b). It is interesting to note that the sonic lines terminate not at the end of the nozzle lips but at the inner wall of the tailpipe, upstream of the jet exit. Thus, the nozzle lip is in supersonic flow. Also, the sonic lines are not straight, as is assumed in one-dimensional flow, but are curved and protrude in the center considerably downstream of the jet-exit plane. (See refs. 4 and 5.) The longest and the most bulbous sonic lines are associated with the smaller pressure ratios in the pressure-ratio range covered in these tests. The longest and most bulbous line indicated is for a pressure ratio of 1.9, which is close to the critical one-dimensional pressure ratio, 1.81.

Distortion of the flow pattern is also indicated by the lack of symmetry in the constant Mach number lines and sonic lines. Difficulty has been experienced in obtaining consistent total-pressure measurements in the plane of the jet exit near the nozzle lip. The supersonic speeds, and perhaps outward-directed angularity of the flow at these points, may explain some of the difficulty. The shape of nozzle lips apparently has an important effect on nozzle-flow patterns, as indicated in reference 6 (pp. 40 and 41).

CONCLUDING REMARKS

An investigation has been made of the jet-exhaust flow-distortion characteristics of several hydrogen peroxide decomposition engines. The total-pressure distribution in the jet exits of 16 engine-simulator configurations was measured under static conditions to determine the influence of various design parameters on flow characteristics.

The contraction ratio of the tailpipe proved to be an effective design parameter in controlling flow distortion. Flow distortion decreased, in general, with increase in contraction ratio. The liquid-propellant distribution plate and catalyst-bed retainer-plate design also affected the flow pattern. The installation of flow-straightener plates in the tailpipes proved to be effective in decreasing flow distortion by increasing total pressures in the center of the jet exits.

Static-pressure and Mach number distribution measurements along the tailpipe were found to be in good agreement with one-dimensional theory.

Langley Research Center,
National Aeronautics and Space Administration,
Langley Station, Hampton, Va., July 3, 1968,
720-01-00-10-23.

REFERENCES

1. Runckel, Jack F.; and Swihart, John M.: A Hydrogen Peroxide Hot-Jet Simulator for Wind-Tunnel Tests of Turbojet-Exit Models. NASA MEMO 1-10-59L, 1959.

2. Runckel, Jack F.; Willis, Conrad M.; and Salters, Leland B., Jr.: Investigation of Catalyst Beds for 98-Percent-Concentration Hydrogen Peroxide. NASA TN D-1808, 1963.

3. Havill, C. Dewey; and Wingrove, Rodney C.: Flight Investigation of a Full-Scale Aircraft Ejector With Various Spacing Ratios and Correlation With Small-Scale Tests. NACA RM A58D21, 1958.

4. Hopkins, D. F.; and Hill, D. E.: Effect of Small Radius of Curvature on Transonic Flow in Axisymmetric Nozzles. AIAA J., vol. 4, no. 8, Aug. 1966, pp. 1337-1343.

5. Oswatitsch, Kl.; and Rothstein, W.: Flow Pattern in a Converging-Diverging Nozzle. NACA TM 1215, 1949.

6. Norton, Harry T., Jr.; Cassetti, Marlowe D.; and Mercer, Charles E.: Transonic Off-Design Performance of a Fixed Divergent Ejector Designed for a Mach Number of 2.0. NASA TM X-165, 1959.

APPENDIX

CATALYST-BED ARRANGEMENTS

The typical catalyst-bed arrangements used in the engine-simulator configurations with diameters of 10.16 cm (4 in.) or larger consisted of the following:

1	distribution plate
1	20-mesh, 0.014 stainless-steel screen
5	20-mesh, 0.014 silver screens
1	antichannel baffle
4 sets	one stainless-steel screen and five silver screens
1	antichannel baffle
12 sets	one stainless-steel screen and five silver screens
40 to 65	20-mesh, 0.014 stainless-steel screens
2	10-mesh, 0.025 stainless-steel screens
1	retainer plate

The typical catalyst-bed arrangements used in engine-simulator configurations IIIA to IIID, which had diameters of 7.34 cm (2.89 in.), consisted of the following:

1	distribution plate
5	20-mesh, 0.014 stainless-steel screens
5	20-mesh, 0.014 silver screens
1	20-mesh, 0.014 stainless-steel screen
1	antichannel baffle
6 sets	one stainless-steel screen and five silver screens
1	antichannel baffle
9 sets	one stainless-steel screen and five silver screens
5	20-mesh, 0.014 silver screens
5	20-mesh, 0.014 stainless-steel screens
2	10-mesh, 0.025 stainless-steel screens
1	retainer plate

Note: The silver screens used in all of the simulators were treated with a 2-percent samarium nitrate solution.

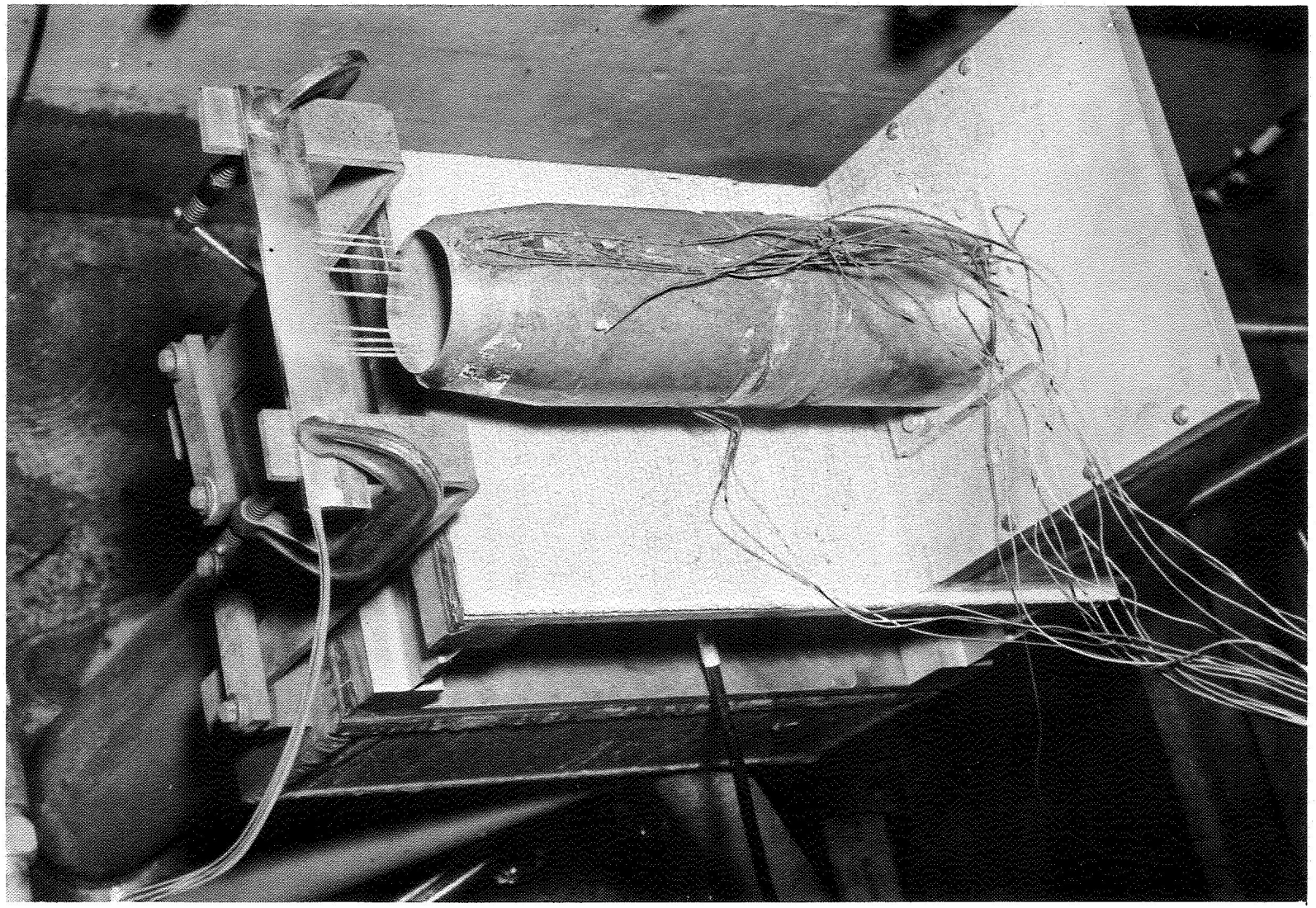

(a) With total-pressure rake. L-64-5390

Figure 1.- Photograph of engine configuration I mounted on thrust balance.

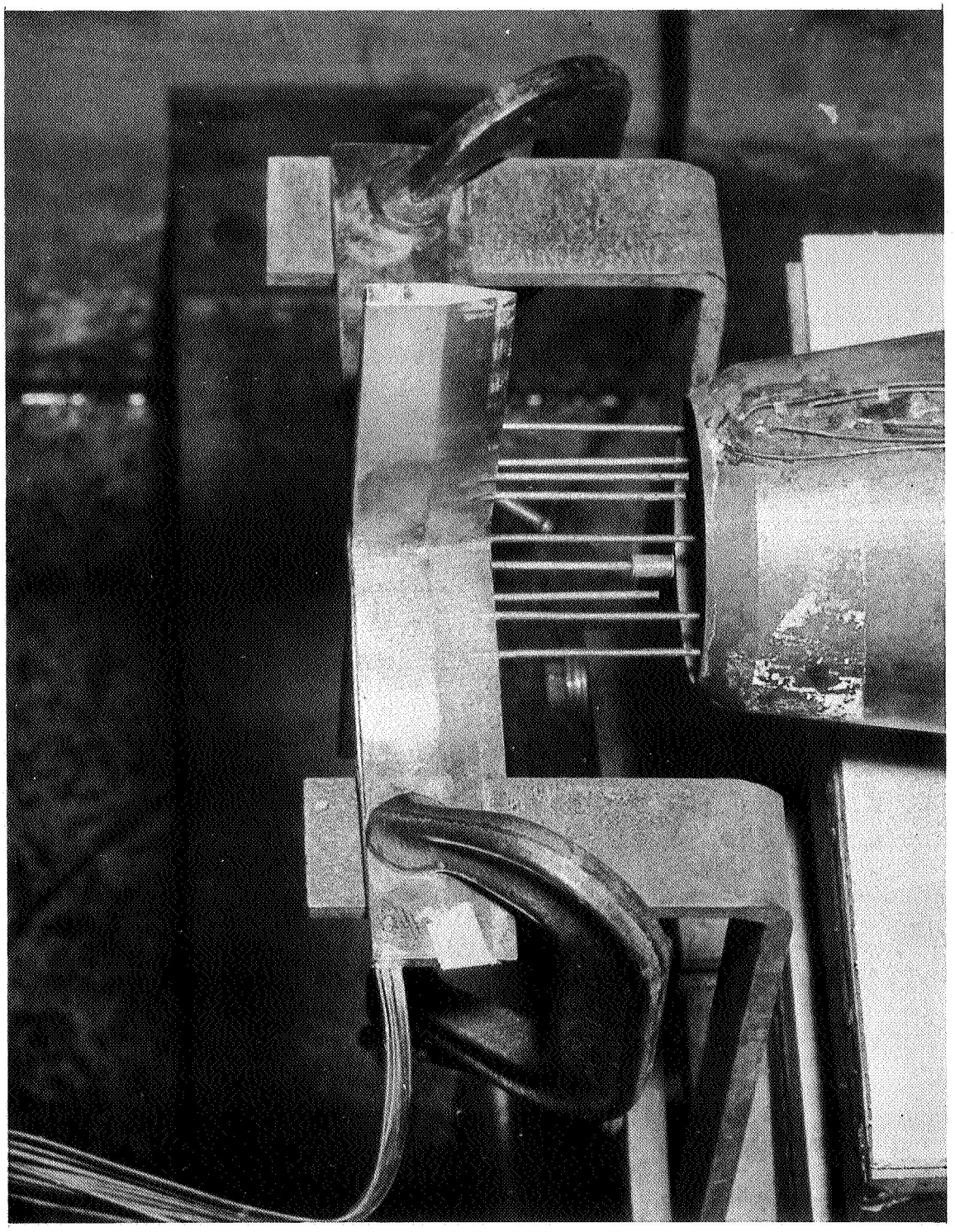

(b) With static-pressure and temperature rake. L-64-5389

Figure 1.- Continued.

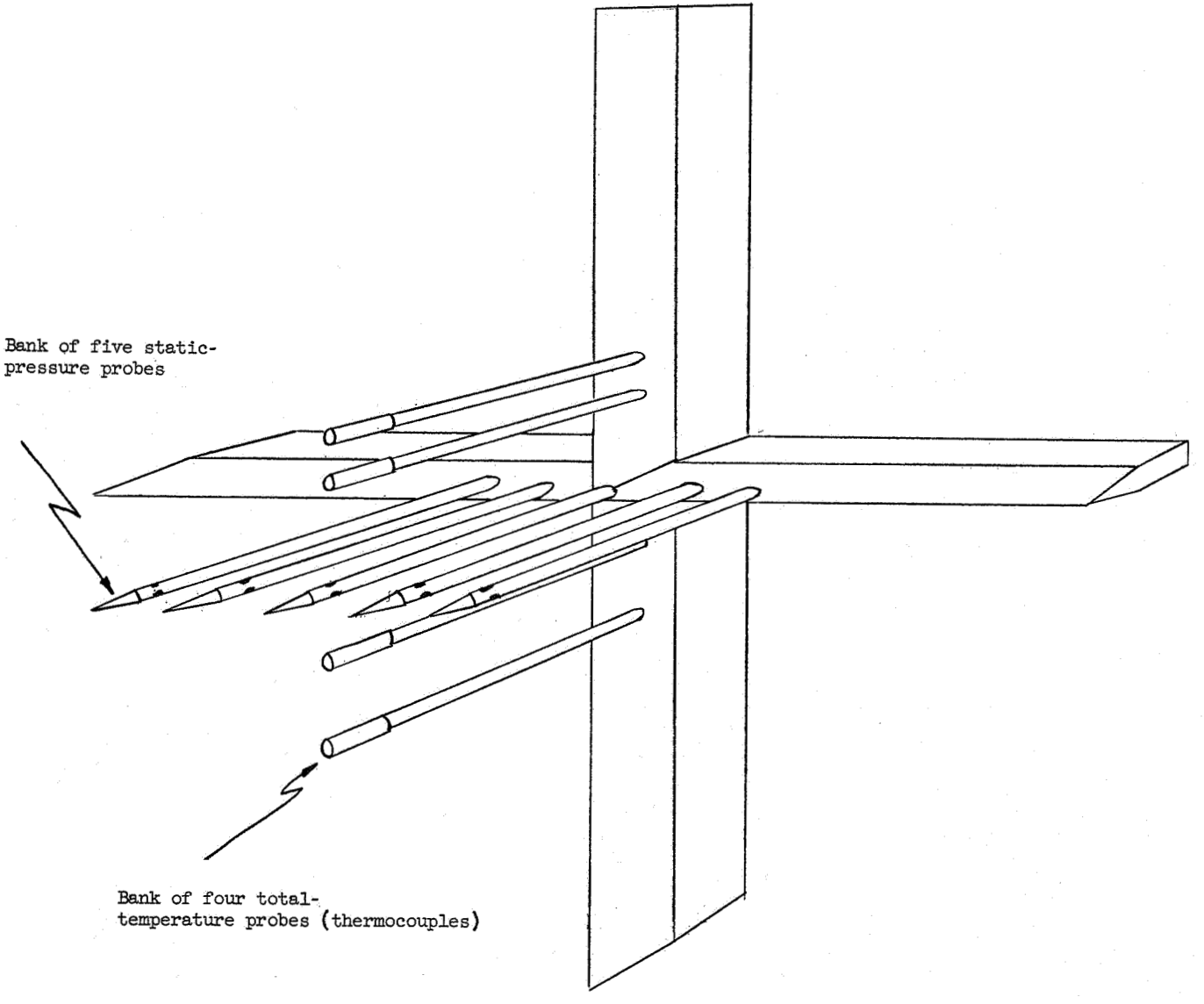

(c) Sketch of cruciform rake used to obtain static pressure and total temperature.

Figure 1.- Concluded.

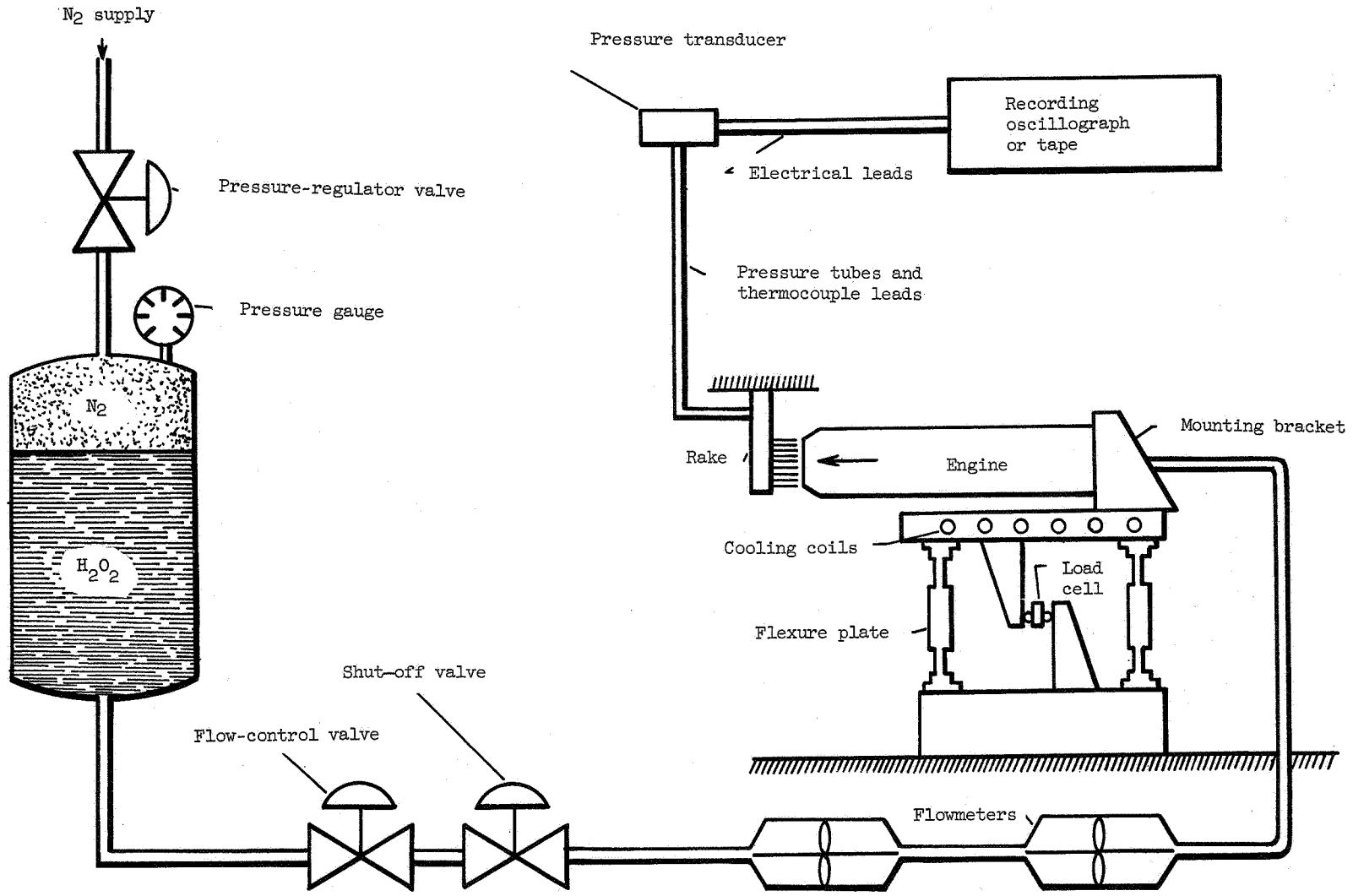

Figure 2.- Schematic diagram of apparatus for flow-distortion studies.

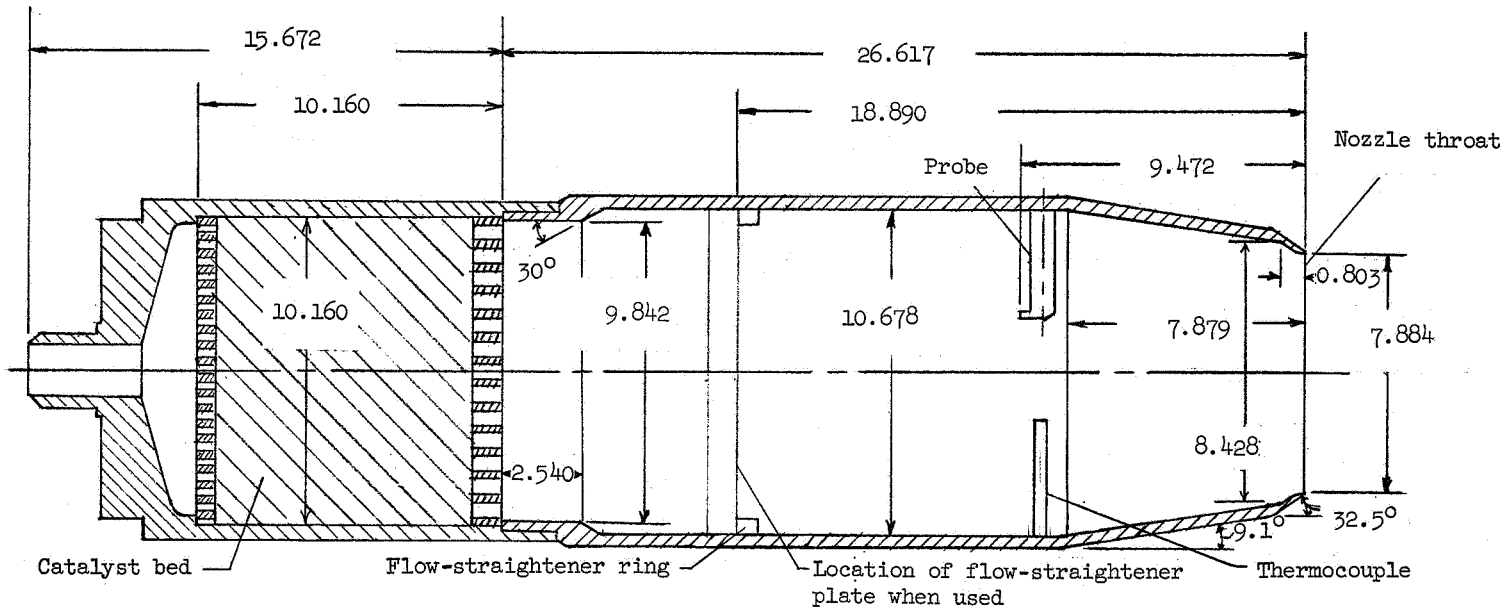

(a) Configurations IA to IE. $A_{max}/A_j = 1.833$.

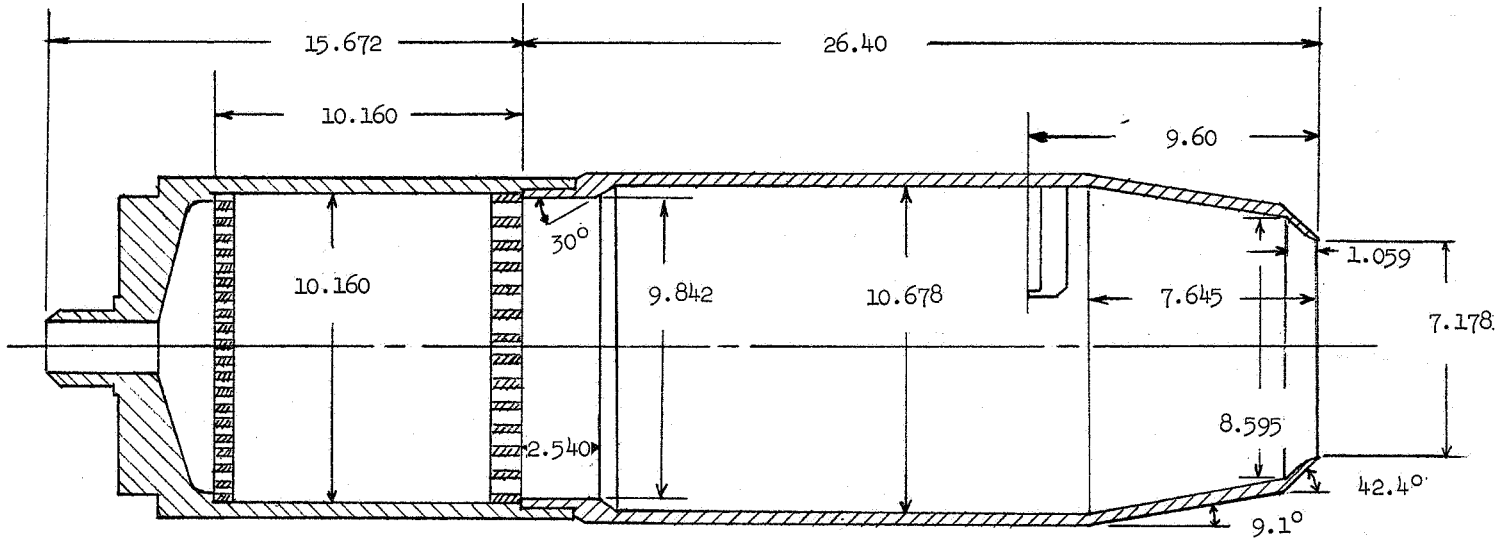

(b) Configuration II. $A_{max}/A_j = 2.215$.

Figure 3.- Schematic diagrams of hydrogen peroxide decomposition engines used in the investigation. Dimensions are in centimeters (1 cm = 0.39366 in.).

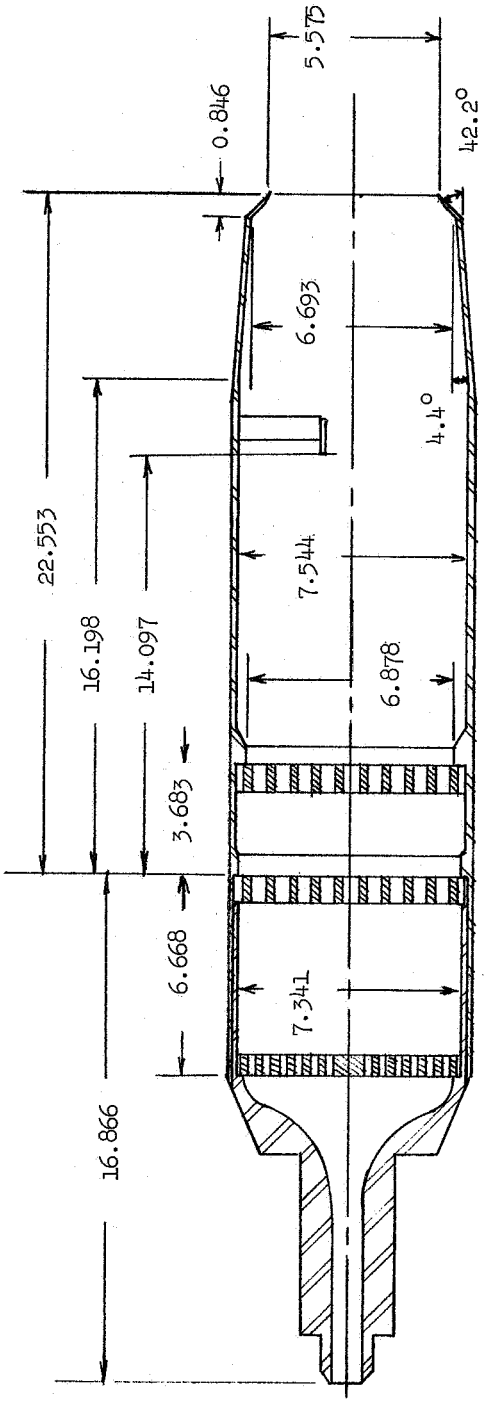

(c) Configuration IIIA. $A_{max}/A_j = 1.827$.

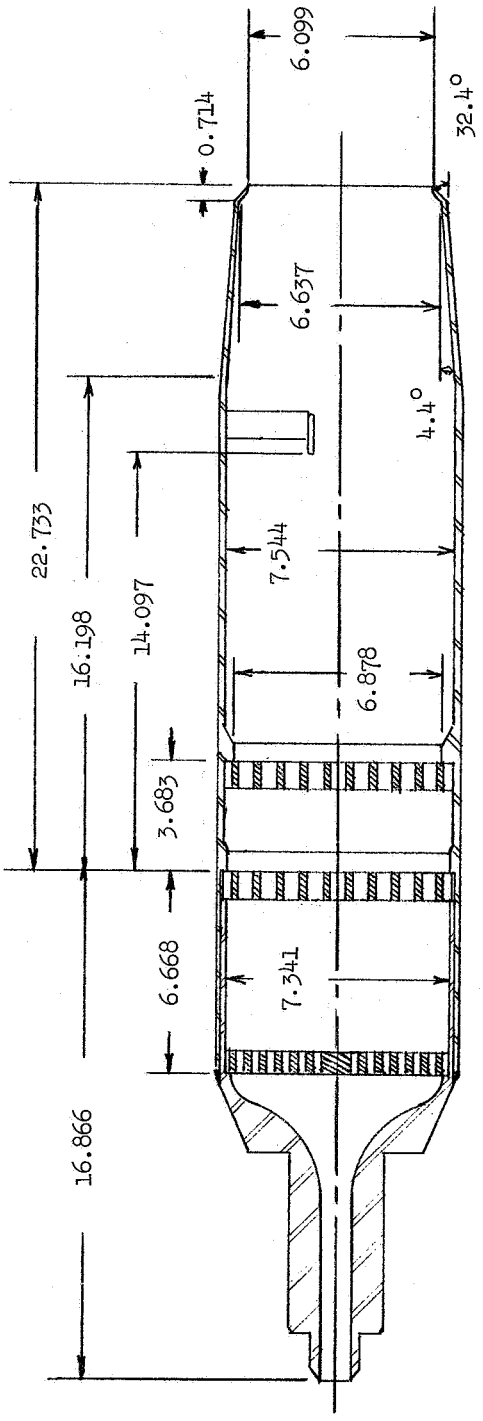

(d) Configuration IIIB. $A_{max}/A_j = 1.532$.

Figure 3.- Continued.

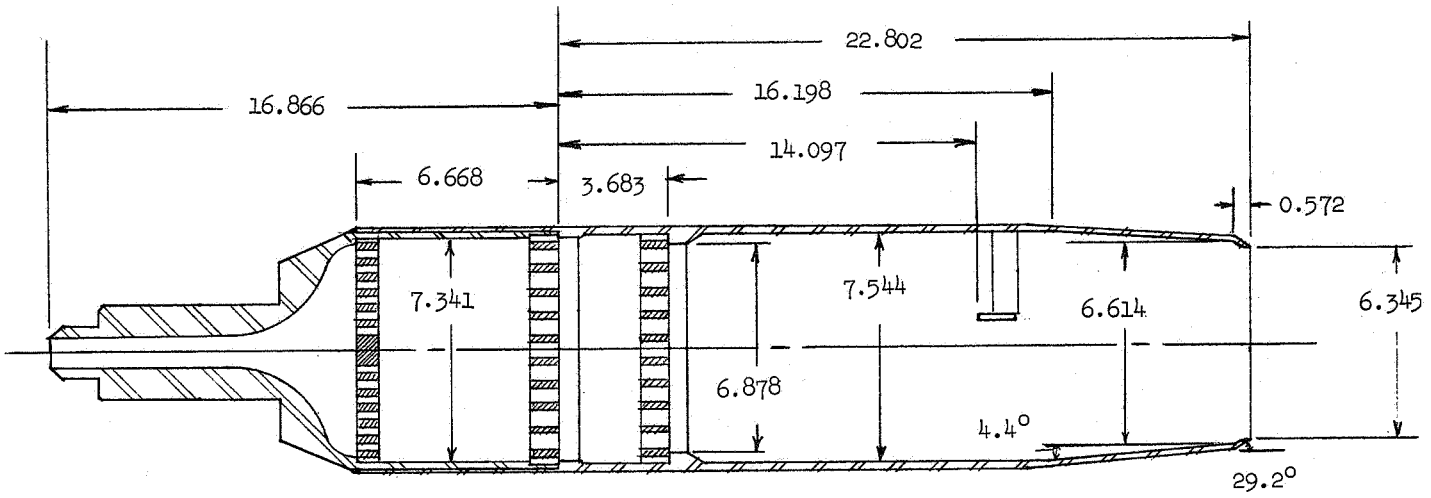

(e) Configuration IIIC. $A_{max}/A_j = 1.413$.

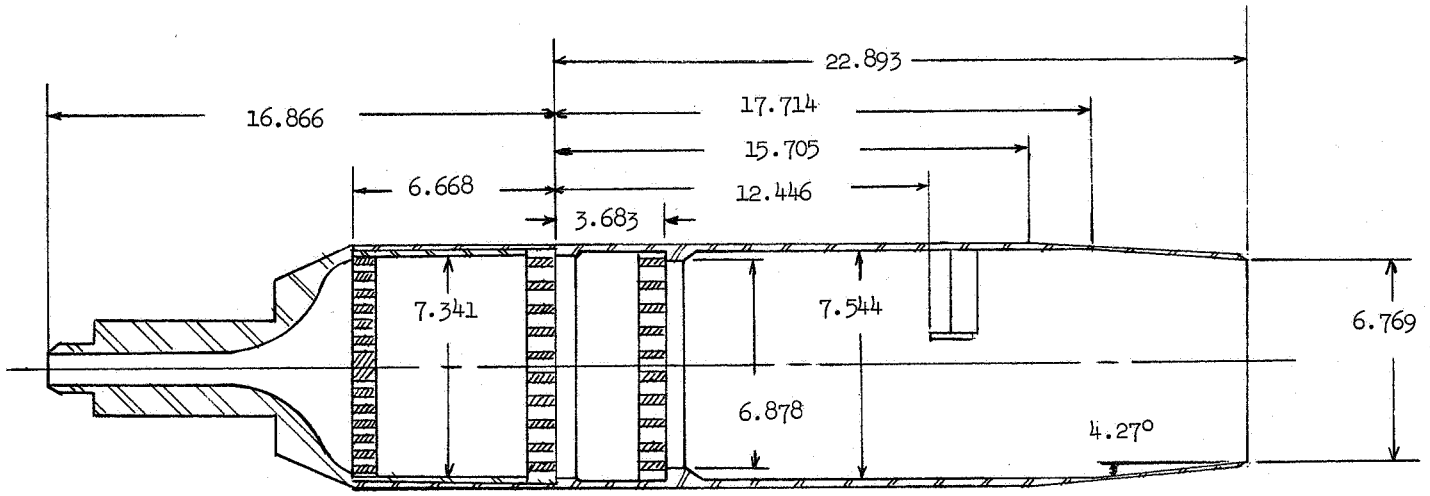

(f) Configuration IIID. $A_{max}/A_j = 1.244$.

Figure 3.- Continued.

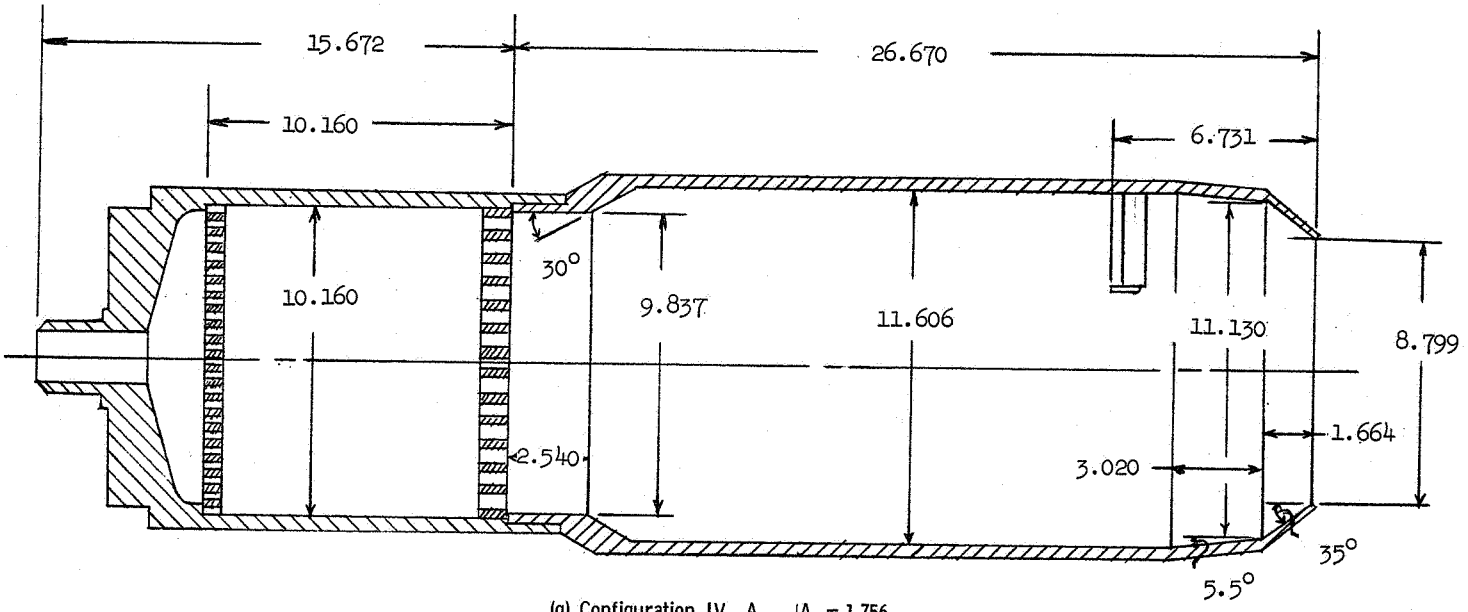

(g) Configuration IV. $A_{max}/A_j = 1.756$.

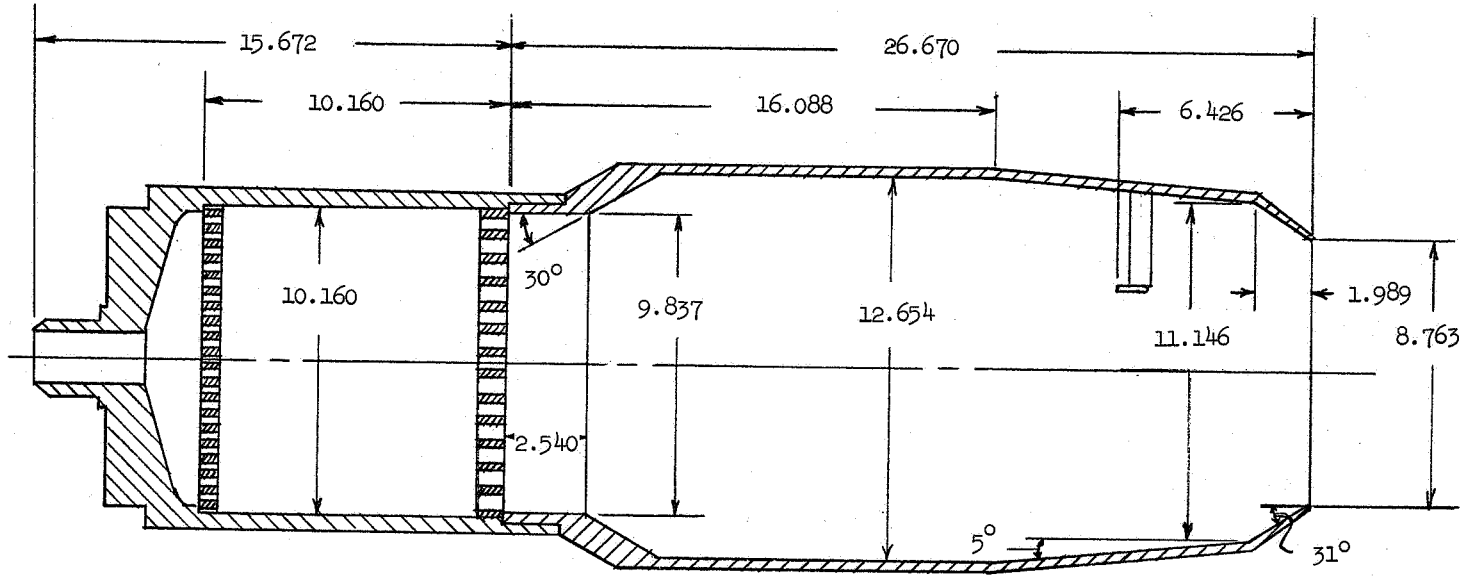

(h) Configuration V. $A_{max}/A_j = 2.088$.

Figure 3.- Continued.

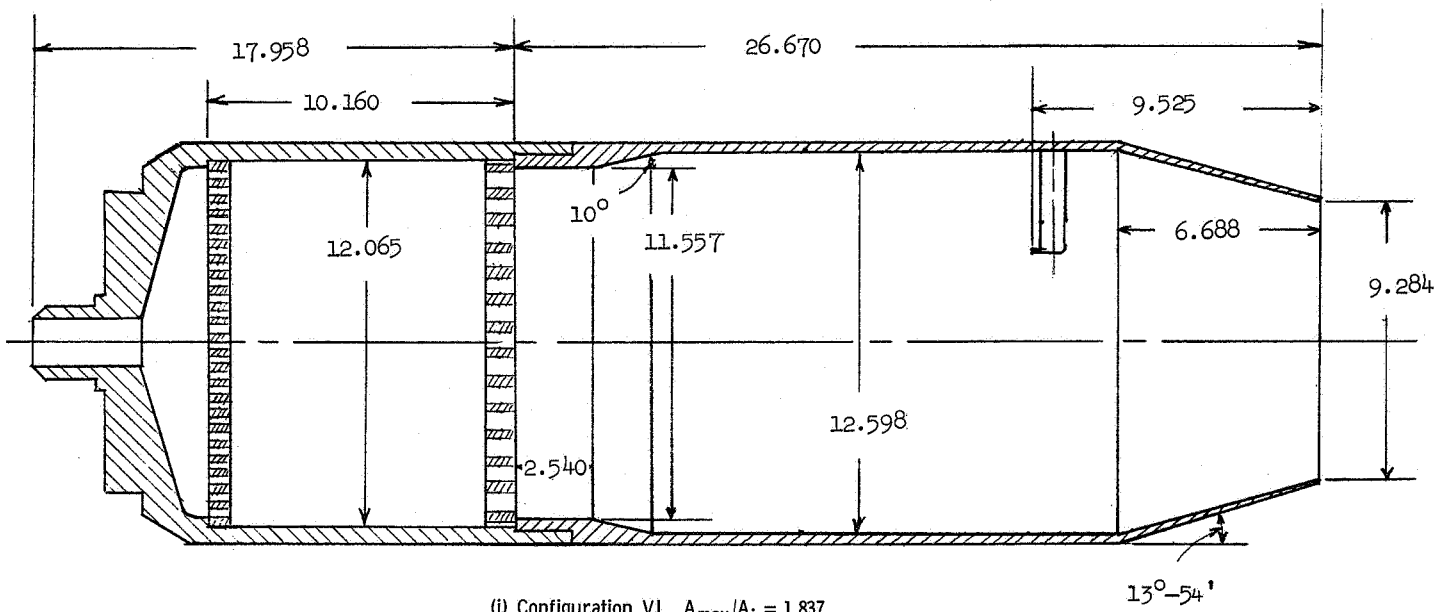

(i) Configuration VI. $A_{max}/A_j = 1.837$.

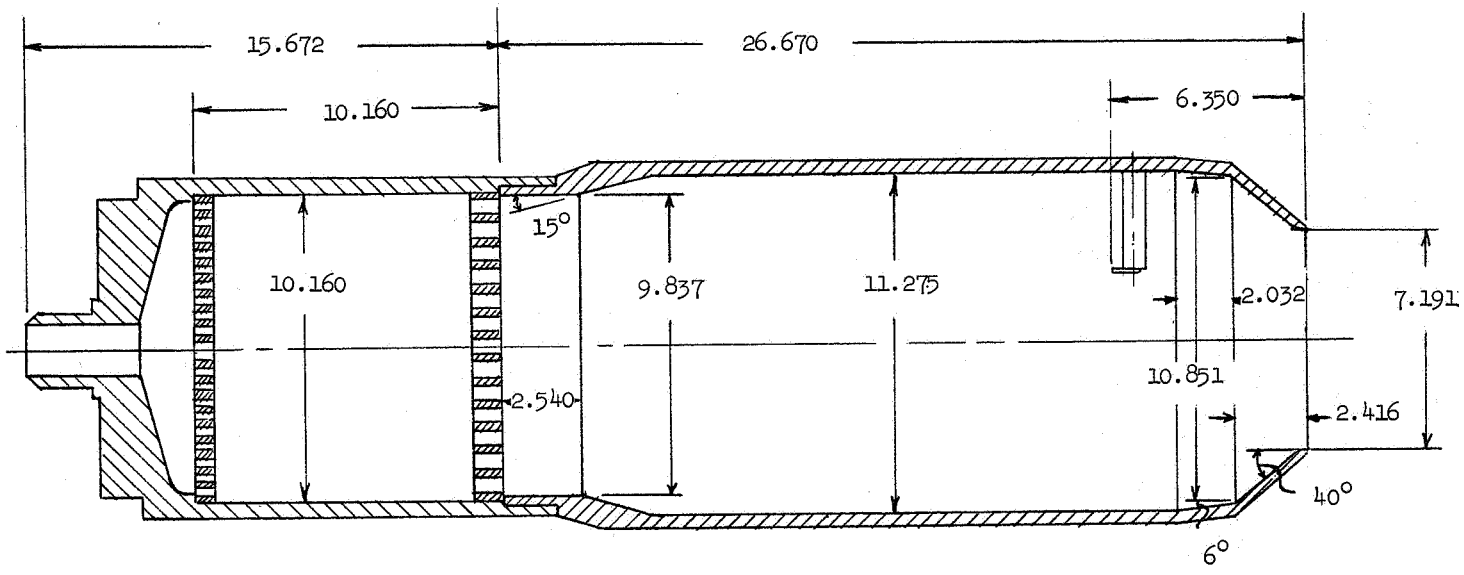

(j) Configuration VII. $A_{max}/A_j = 2.459$.

Figure 3.- Continued.

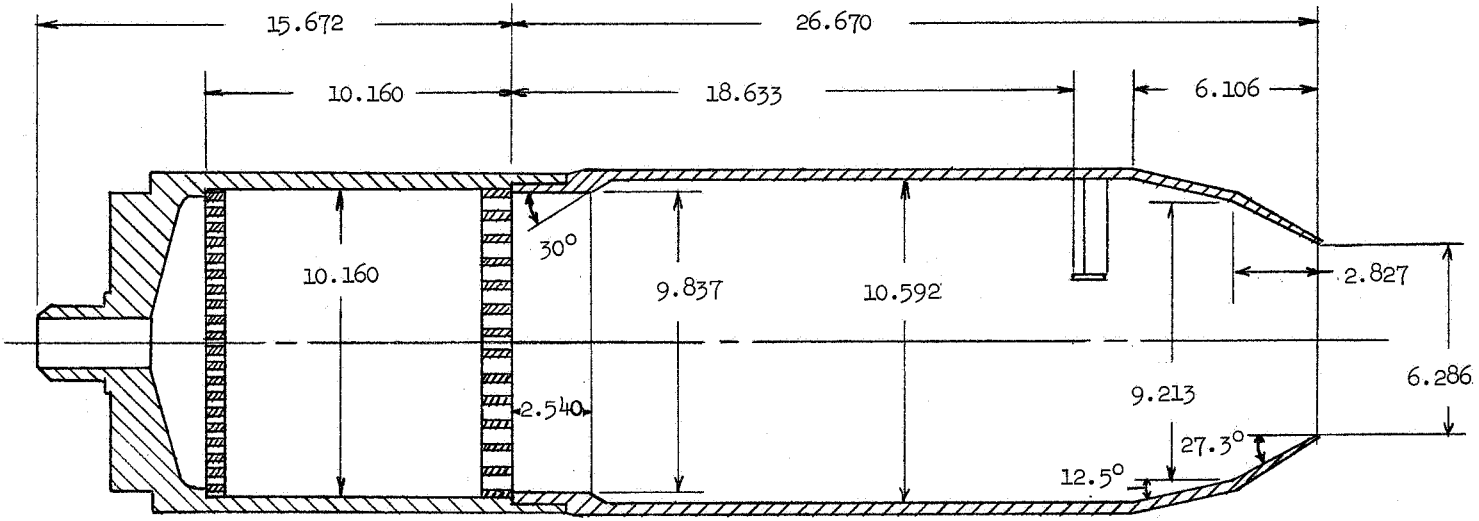

(k) Configuration VIII. $A_{max}/A_j = 2.833$.

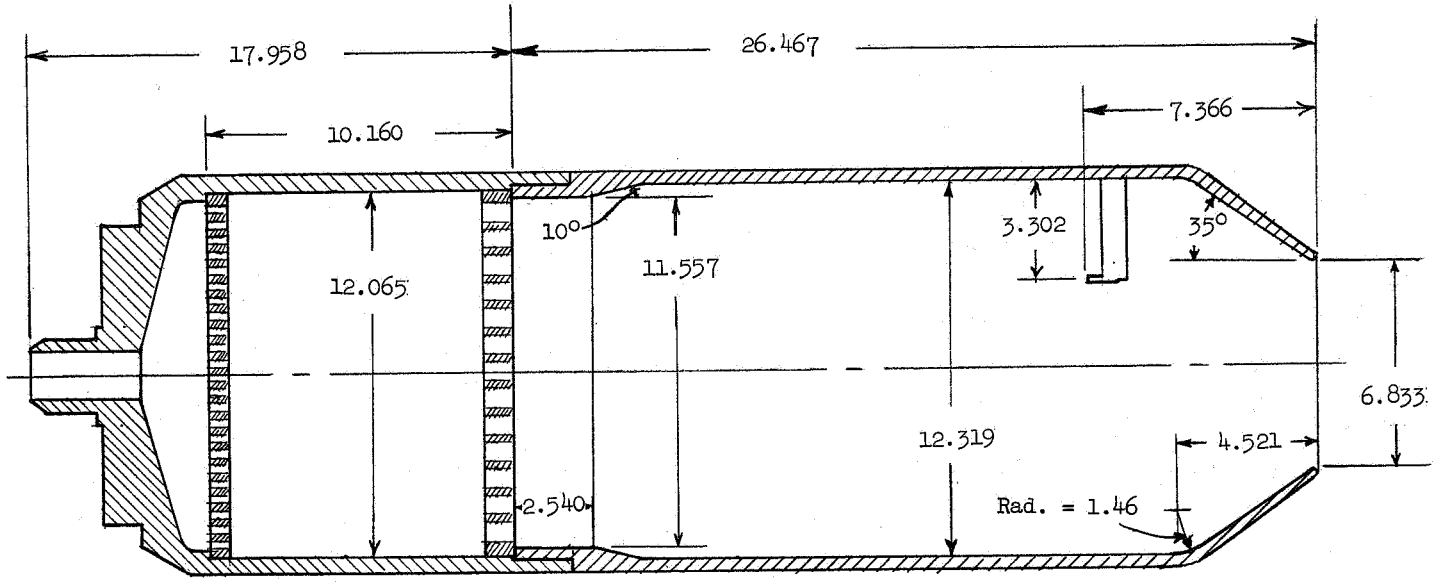

(l) Configuration IX. $A_{max}/A_j = 3.248$.

Figure 3.- Concluded.

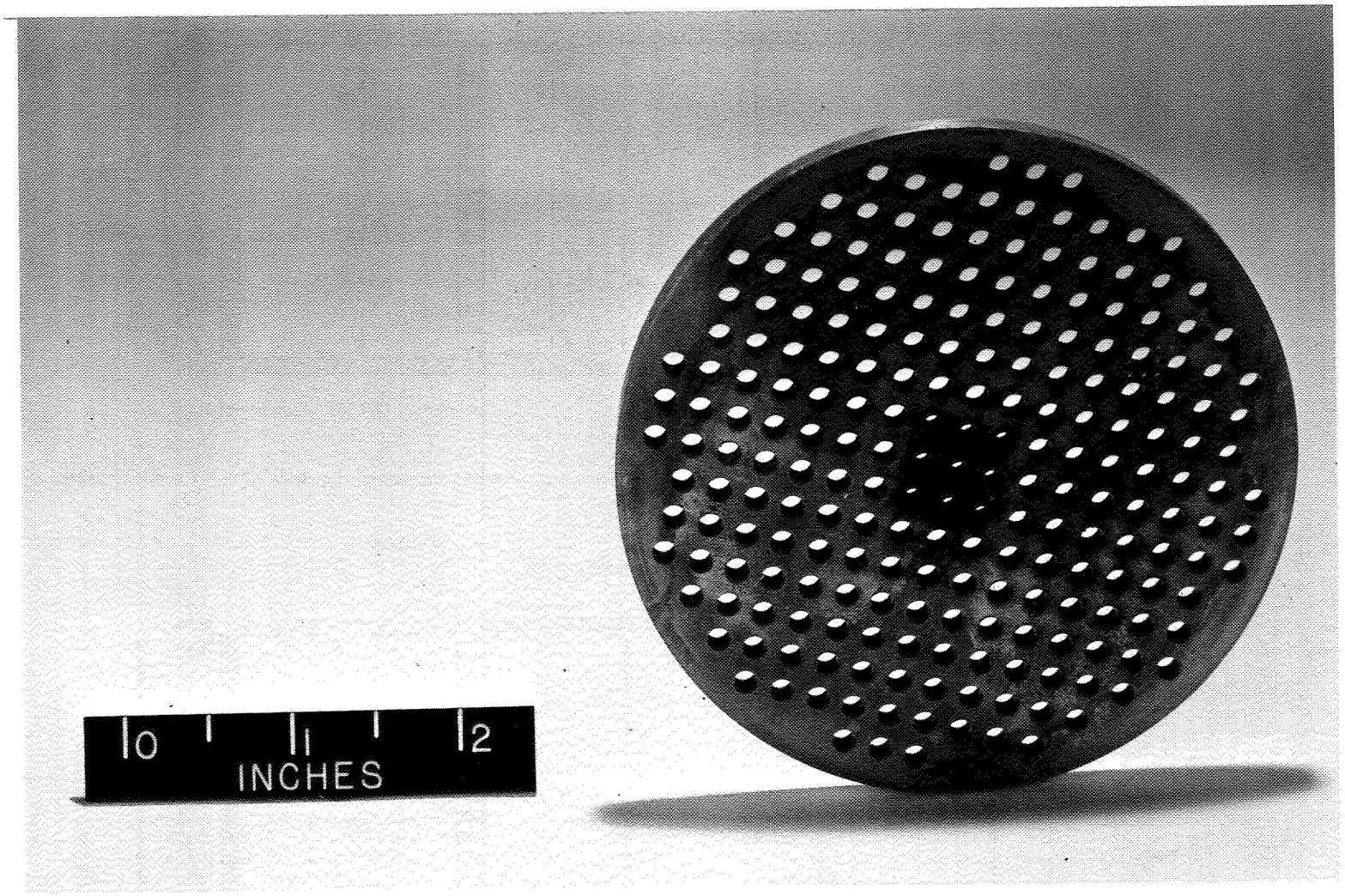

(a) Distribution plate. Open area, 25.6 percent. L-64-5751

Figure 4.- Photographs of several components used in configuration 1.

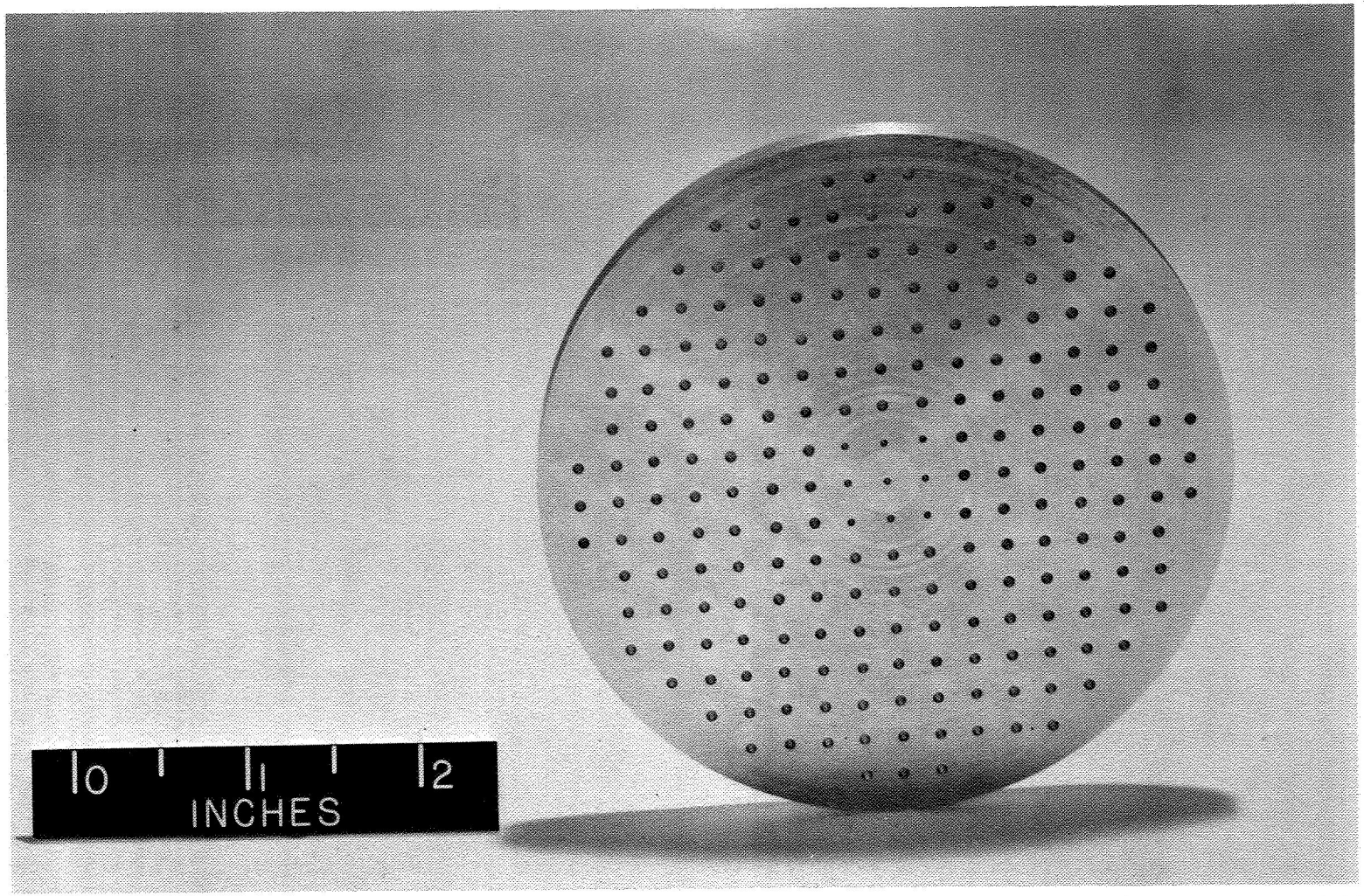

(b) Distribution plate. Open area, 5.2 percent. L-64-5750

Figure 4.- Continued.

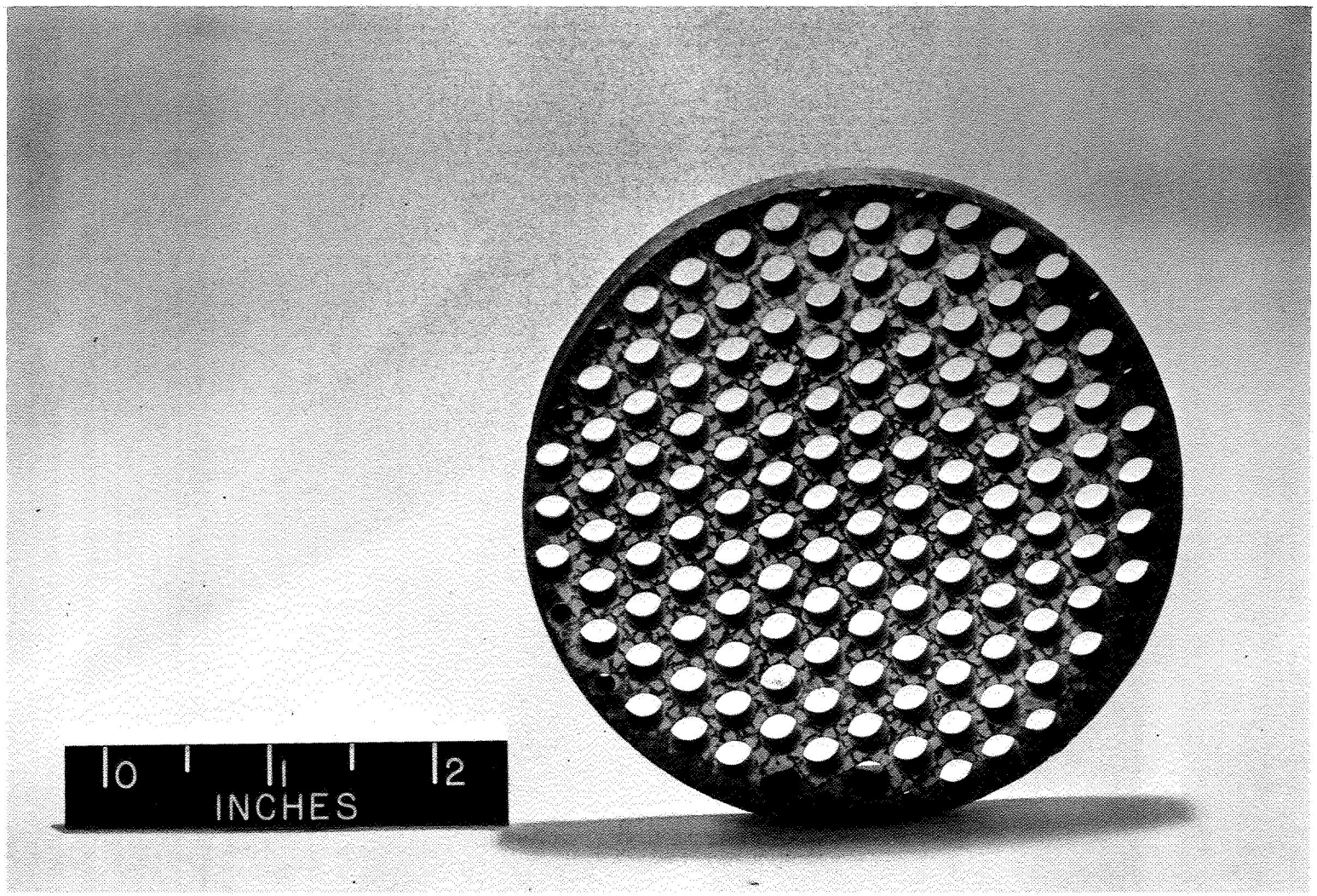

(c) Retainer plate. Open area, 48.7 percent. L-64-5752

Figure 4.- Continued.

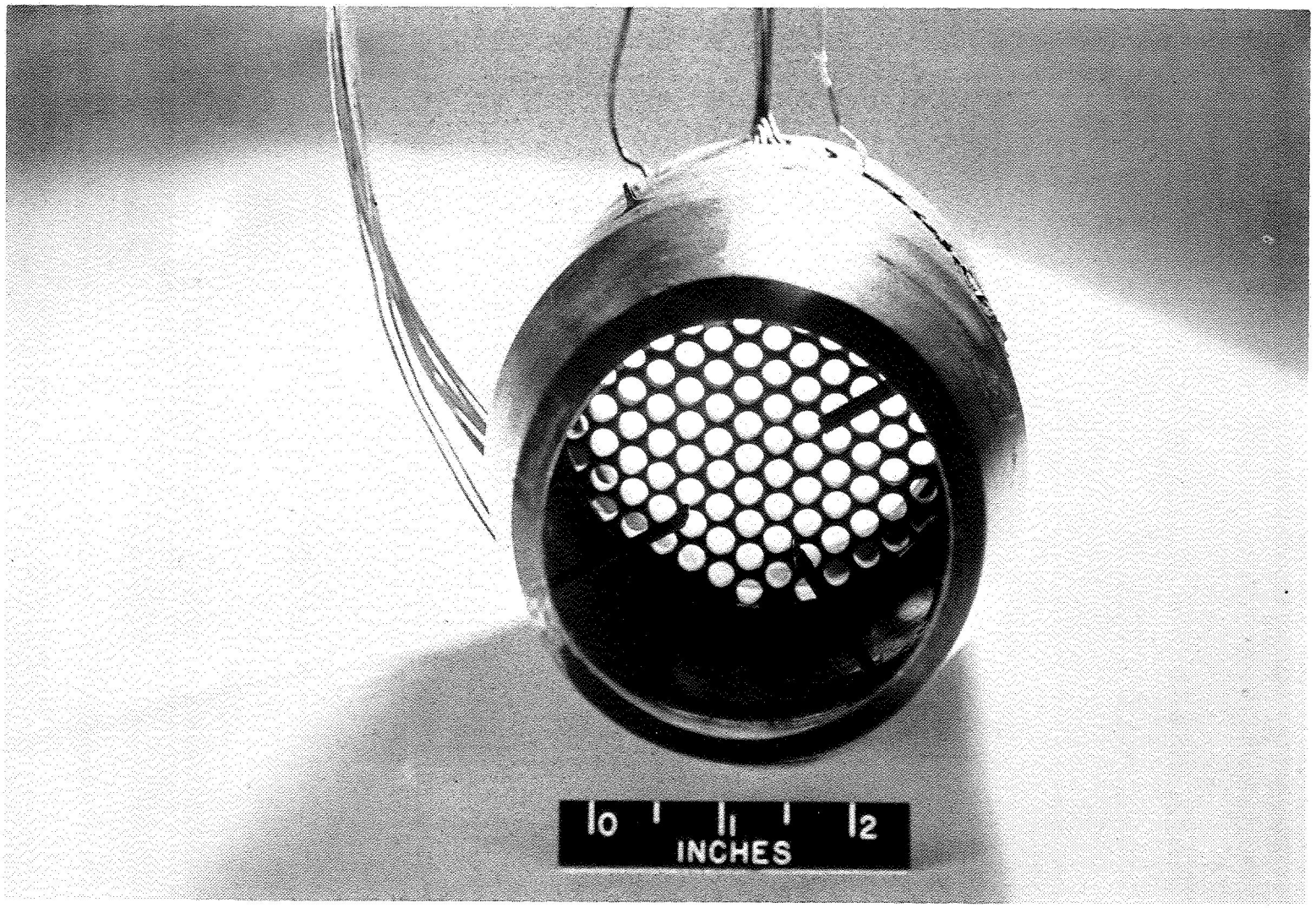

(d) Flow-straightener plate installed in engine tailpipe. Open area, 46.7 percent. L-64-5754

Figure 4.- Concluded.

Figure 5.- Typical 10.16-cm (4-in.) diameter catalyst-bed arrangement after approximately 4 hours operating time with 90-percent hydrogen peroxide (flow from top to bottom). L-63-3870

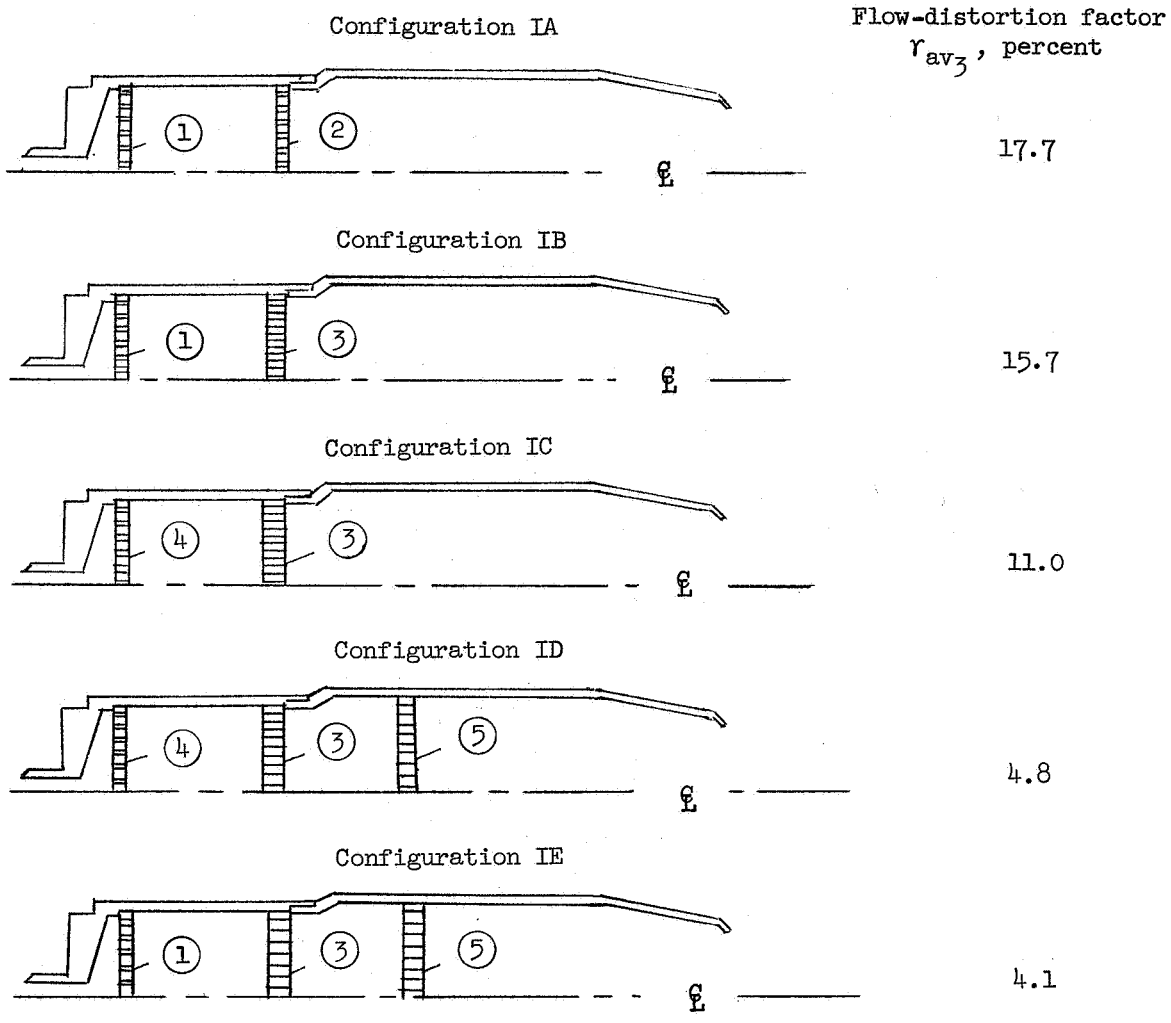

	Item	Open area, percent	Plate thickness in.	cm
(1)	Distribution plate	25.6	0.25	0.635
(2)	Retainer plate	48.7	0.25	0.635
(3)	Retainer plate	48.7	0.375	0.952
(4)	Distribution plate	5.2	0.25	0.635
(5)	Flow-straightener plate	46.7	0.375	0.952

Figure 6.- Average flow-distortion factor for various gas-generator components of configurations IA to IE.

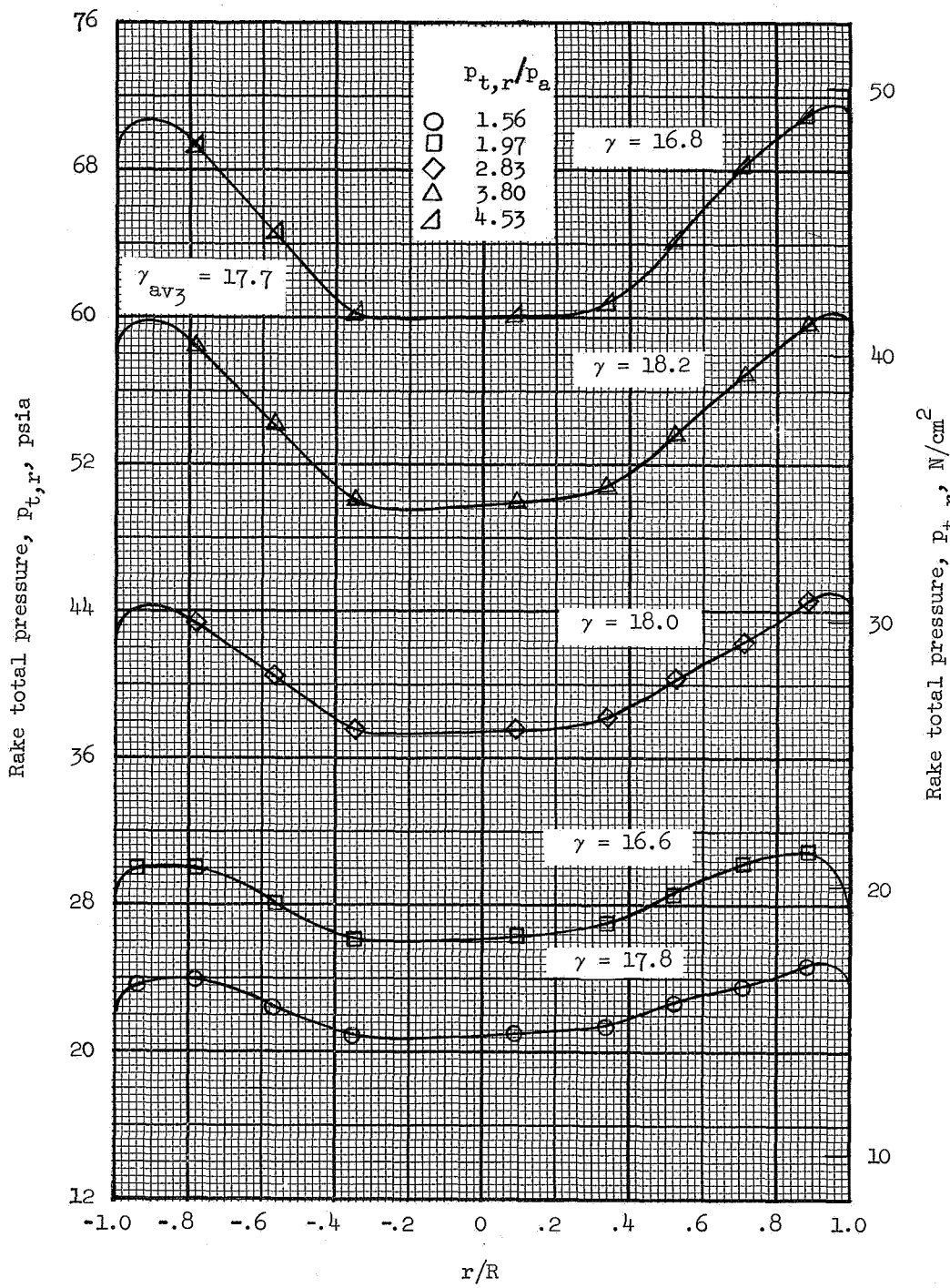

(a) Configuration IA; distribution plate 25.6 percent open, 0.635 cm (0.250 in.) thick; retainer plate, 48.7 percent open, 0.635 cm (0.250 in.) thick.

Figure 7.- Effect of variation of decomposition chamber and tailpipe internal components on total-pressure distributions in jet exit. (Flow-distortion factors in percent.)

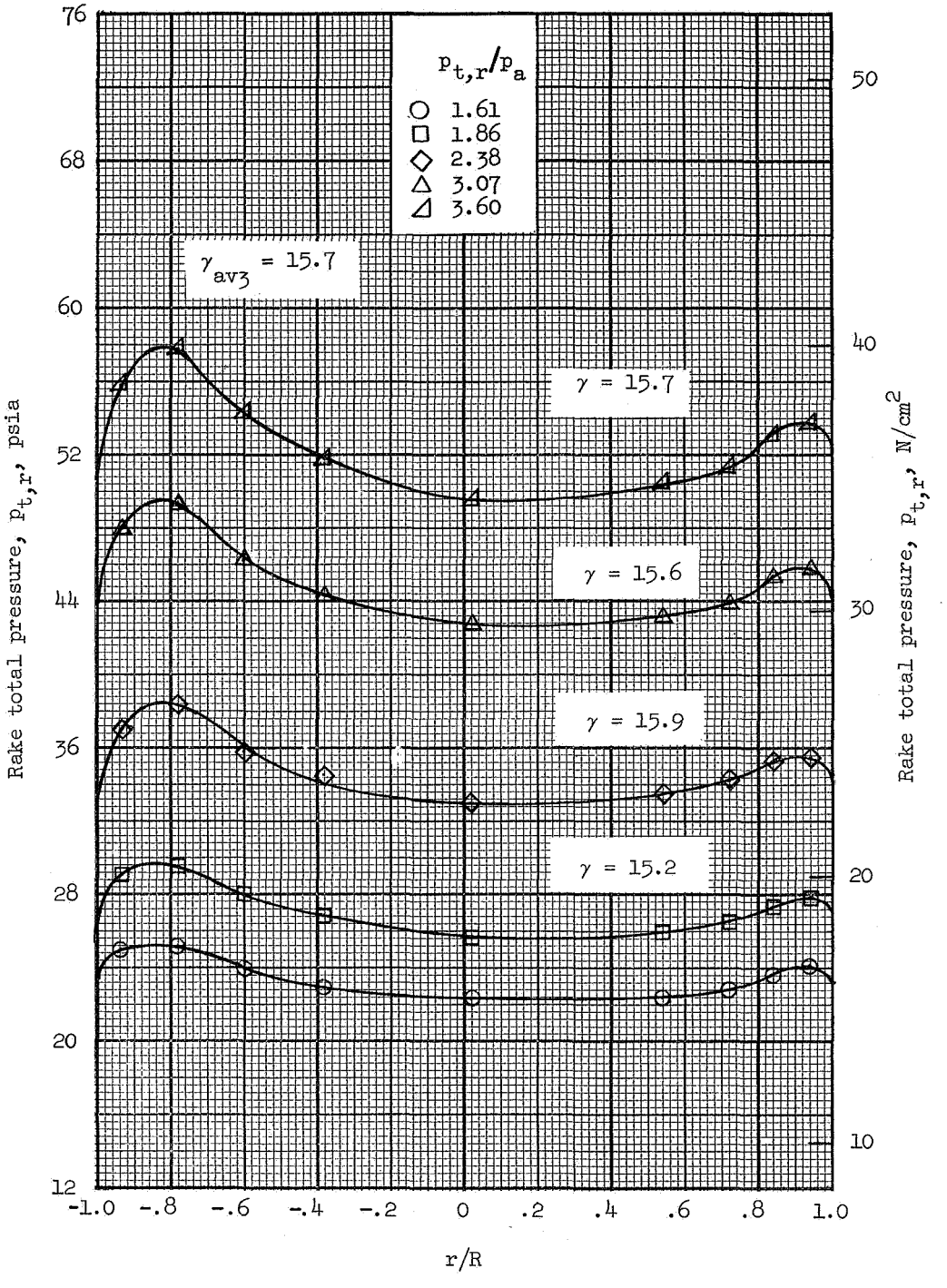

(b) Configuration IB; distribution plate 25.6 percent open, 0.635 cm (0.250 in.) thick; retainer plate, 48.7 percent open, 0.952 cm (0.375 in.) thick.

Figure 7.- Continued.

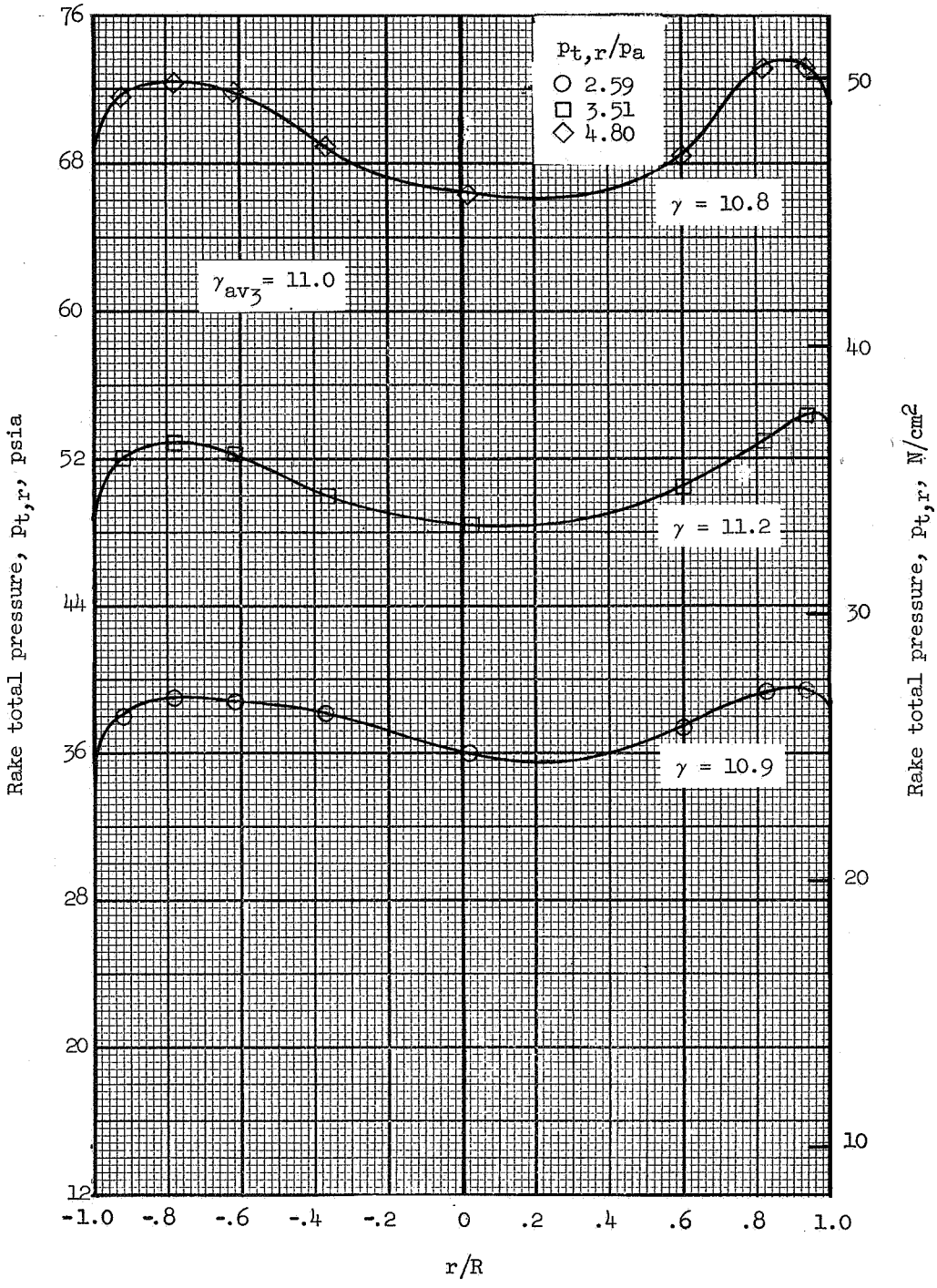

(c) Configuration IC; distribution plate 5.2 percent open, 0.635 cm (0.250 in.) thick; retainer plate, 48.7 percent open, 0.952 cm (0.375 in.) thick.

Figure 7.- Continued.

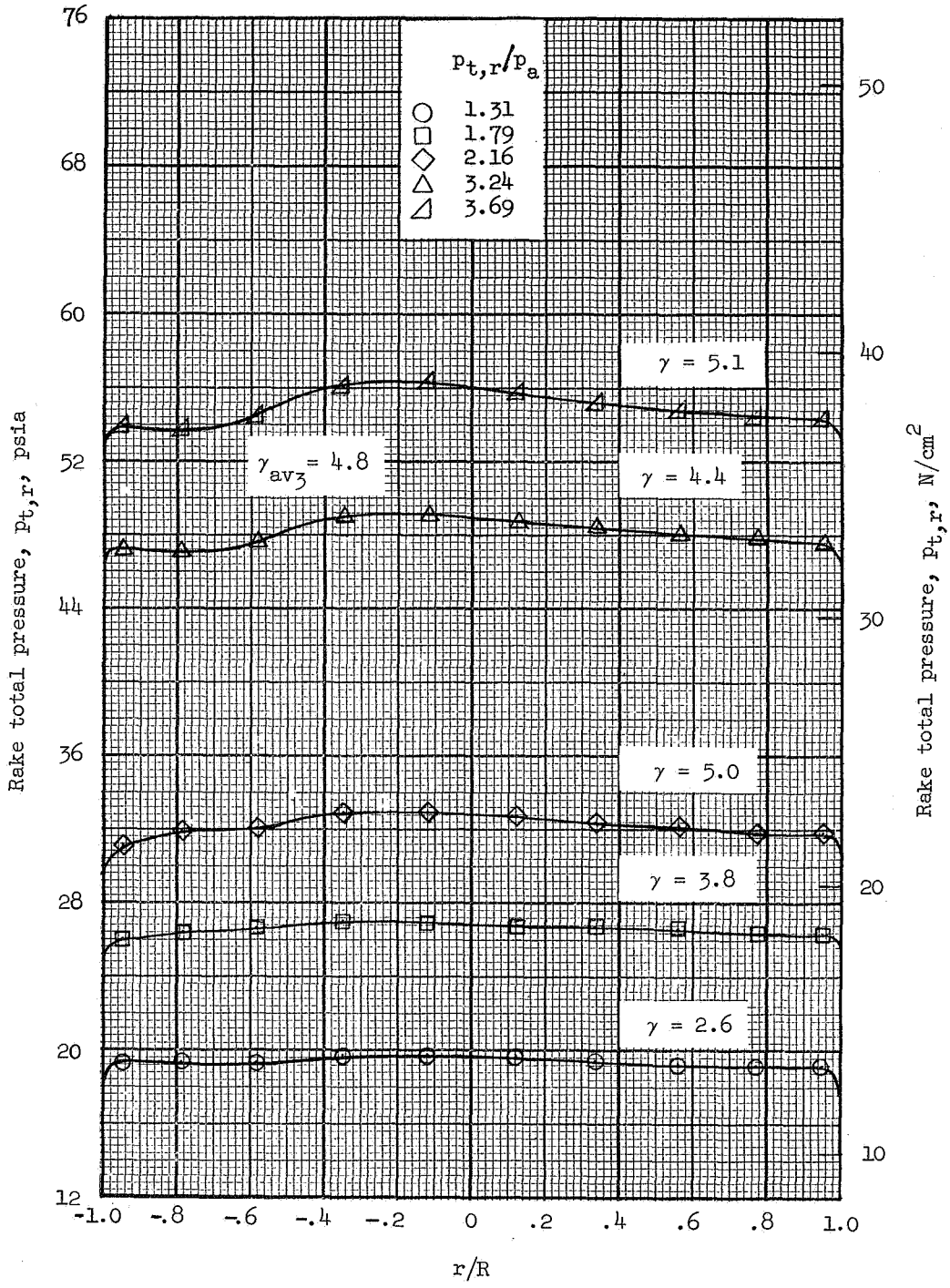

(d) Configuration ID. (Has flow-straightener plate; otherwise identical to configuration IC.)

Figure 7.- Continued.

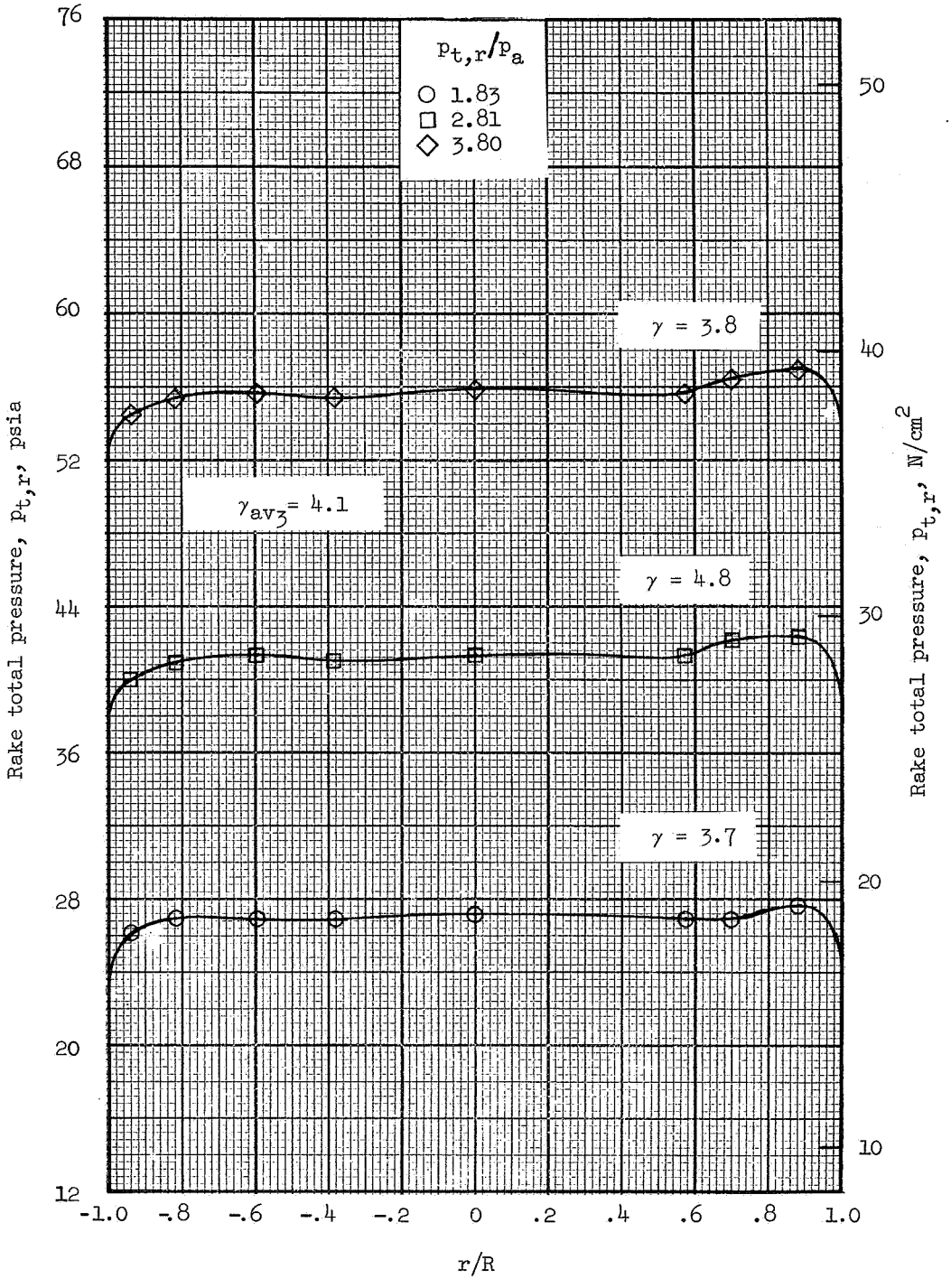

(e) Configuration IE. (Has flow-straightener plate; otherwise identical to configuration IB.)

Figure 7.- Concluded.

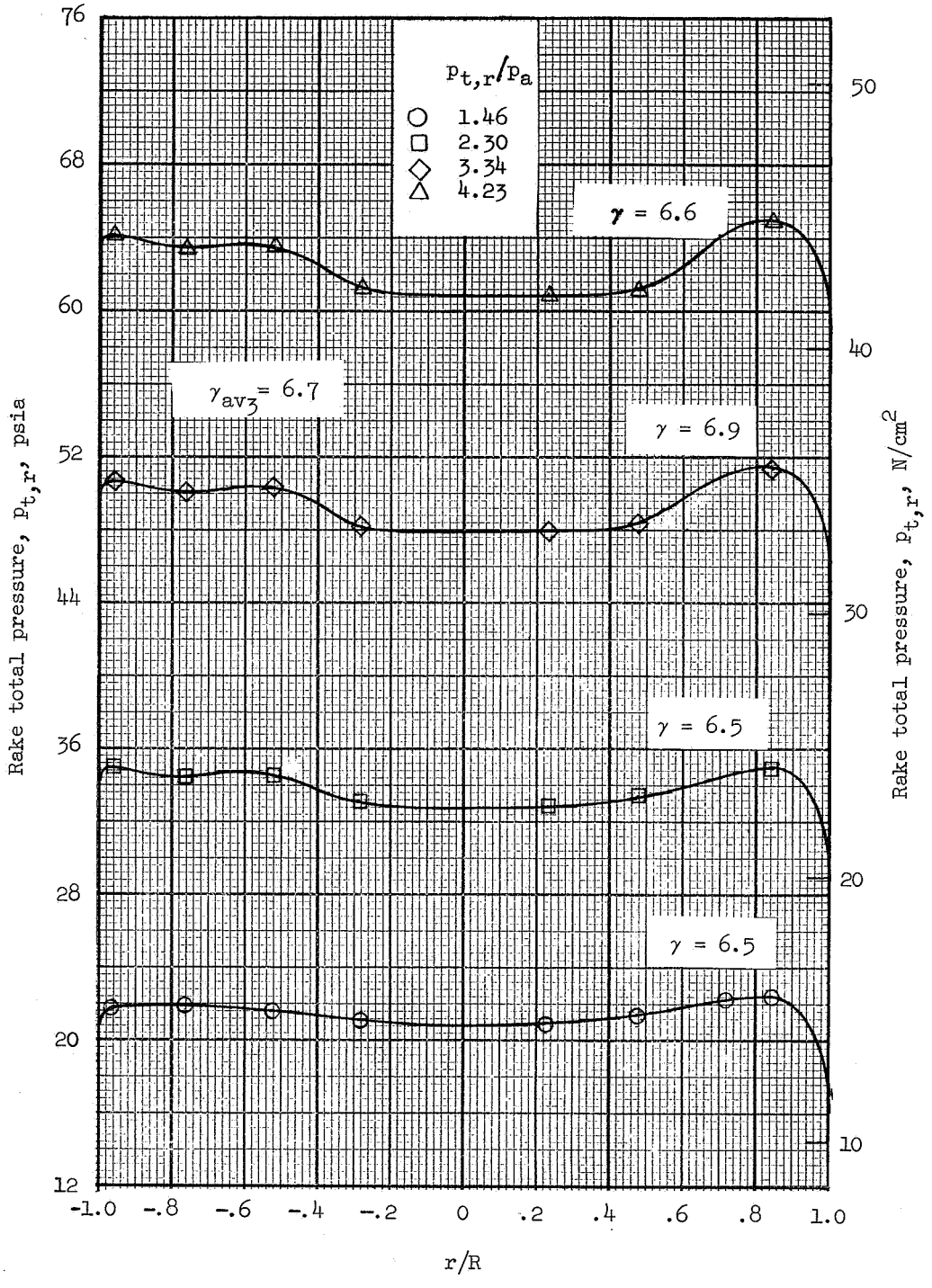

(a) Configuration II.

Figure 8.- Total-pressure distributions in the jet exit of several hydrogen peroxide decomposition engines. (Flow-distortion factors in percent.)

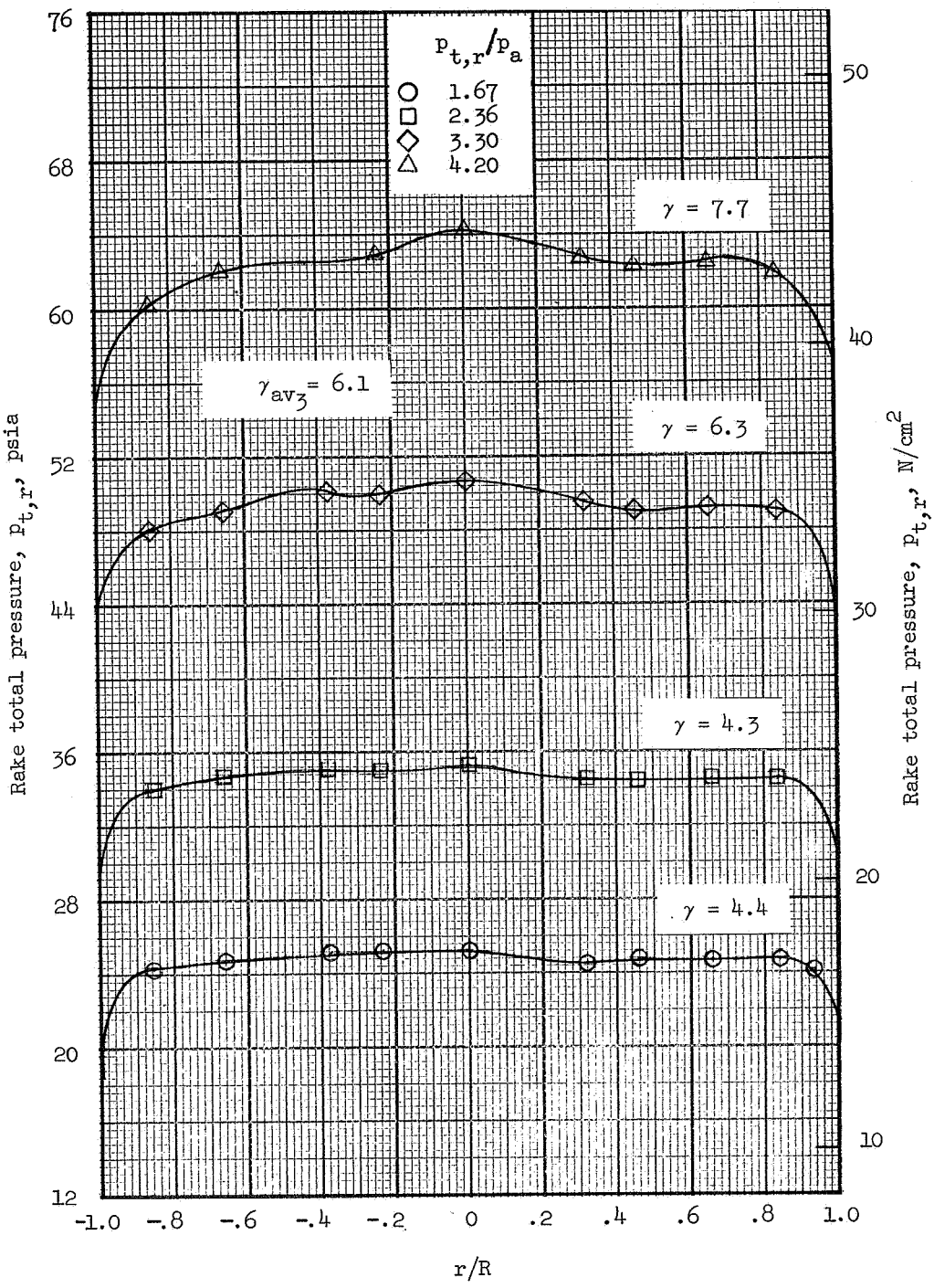

(b) Configuration IIIA.

Figure 8.- Continued.

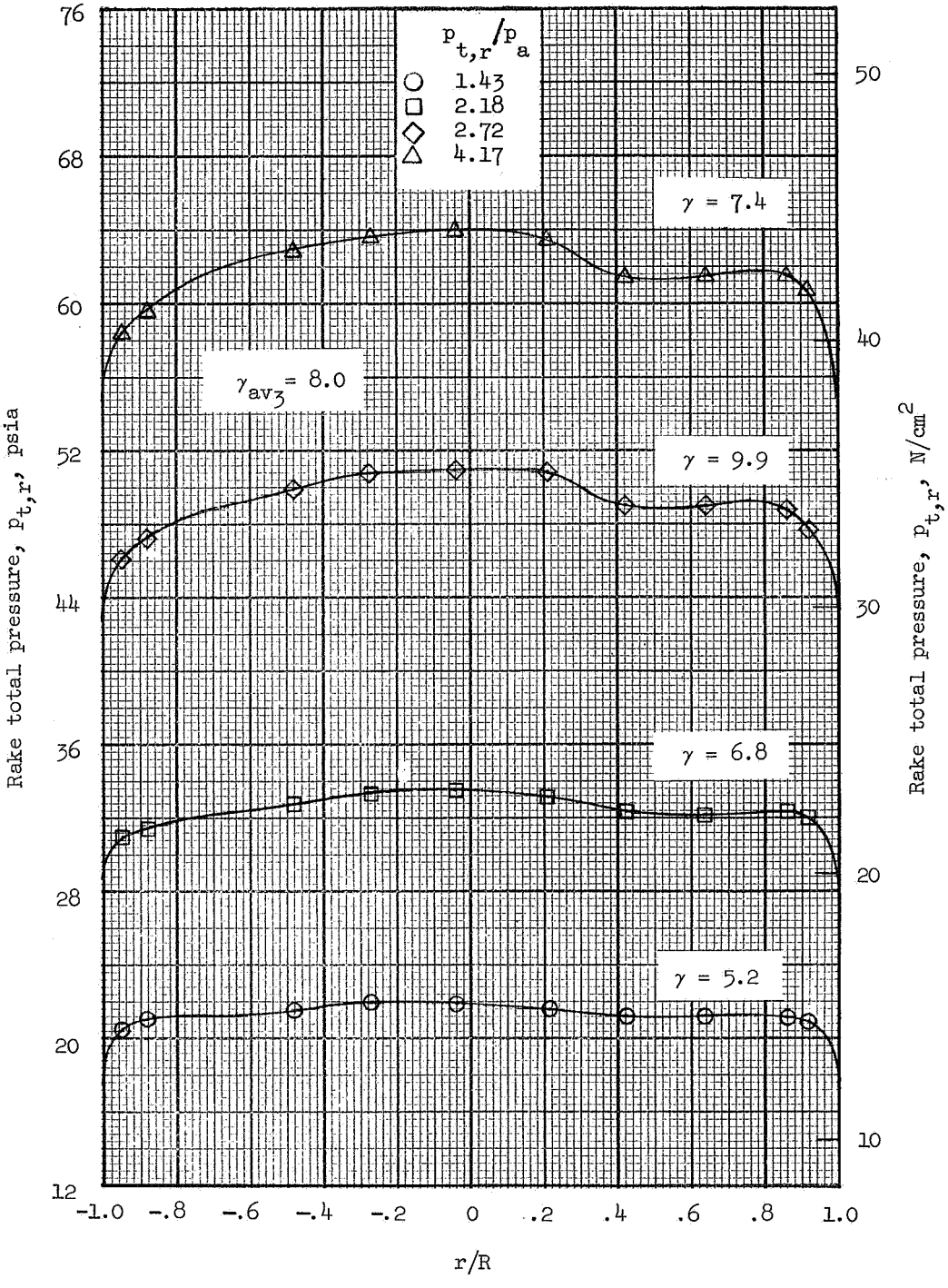

(c) Configuration 111B. Engine 1.

Figure 8.- Continued.

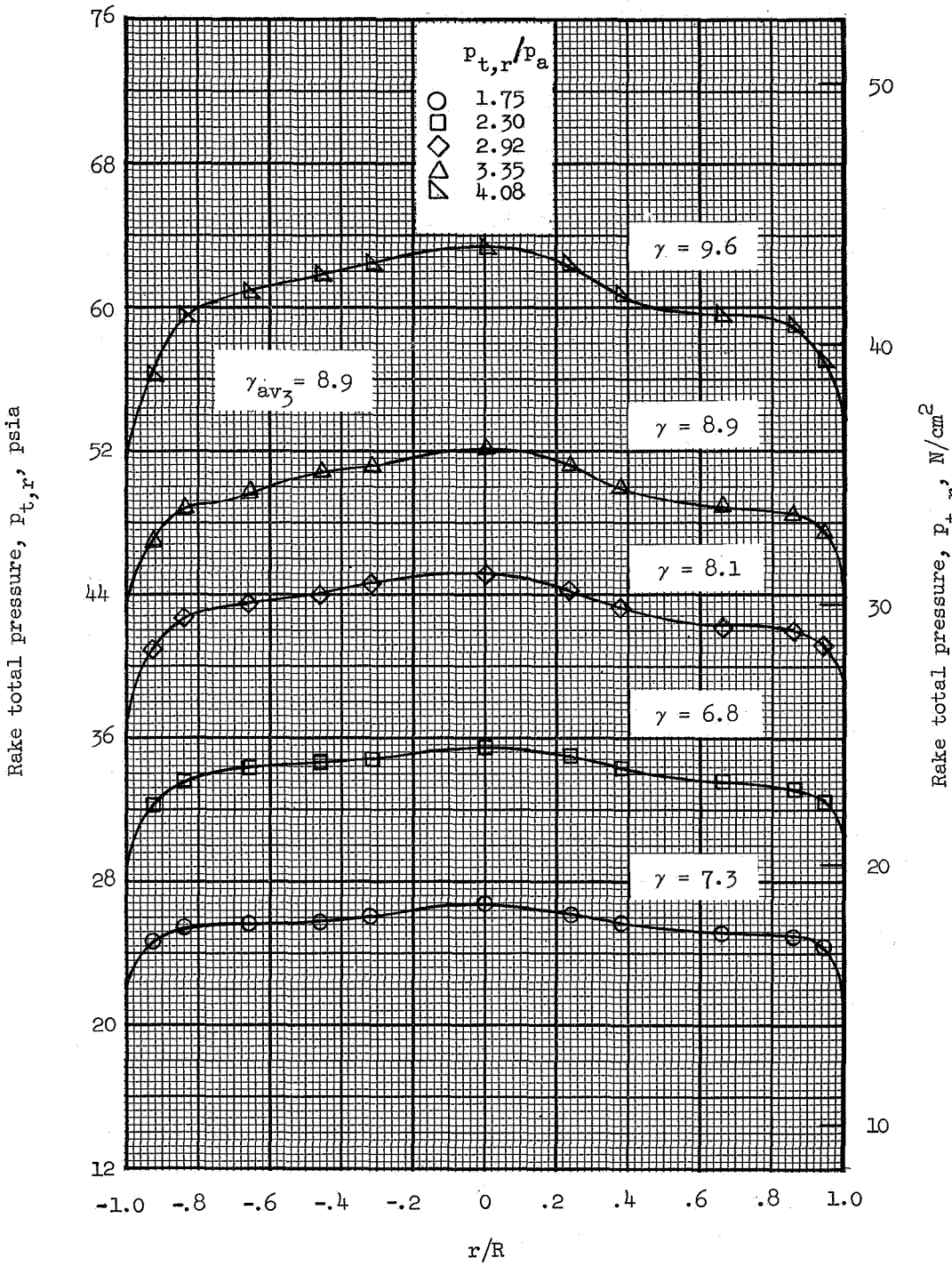

(d) Configuration 111B. Engine 2.

Figure 8.- Continued.

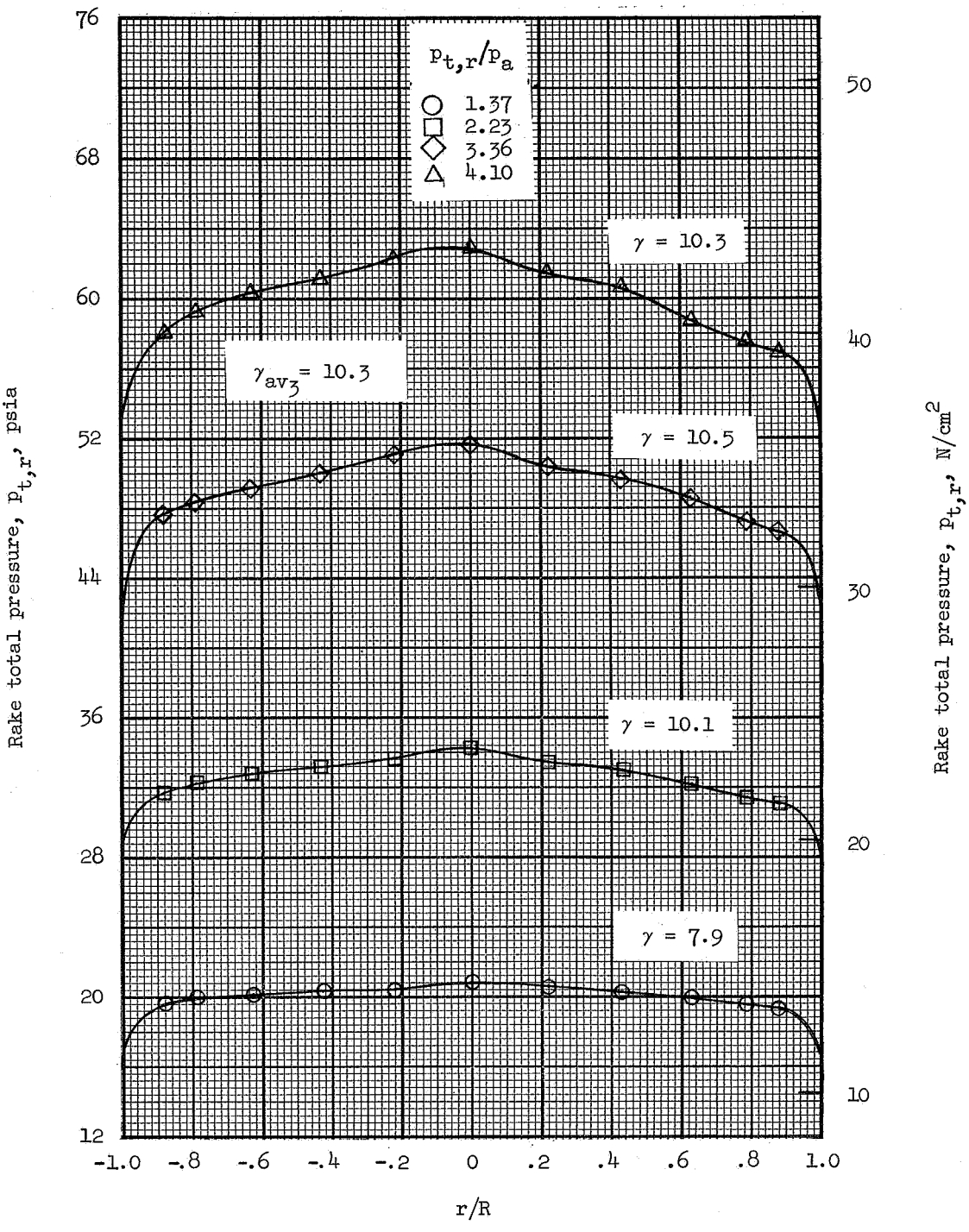

(e) Configuration IIIC. Engine 1.

Figure 8.- Continued.

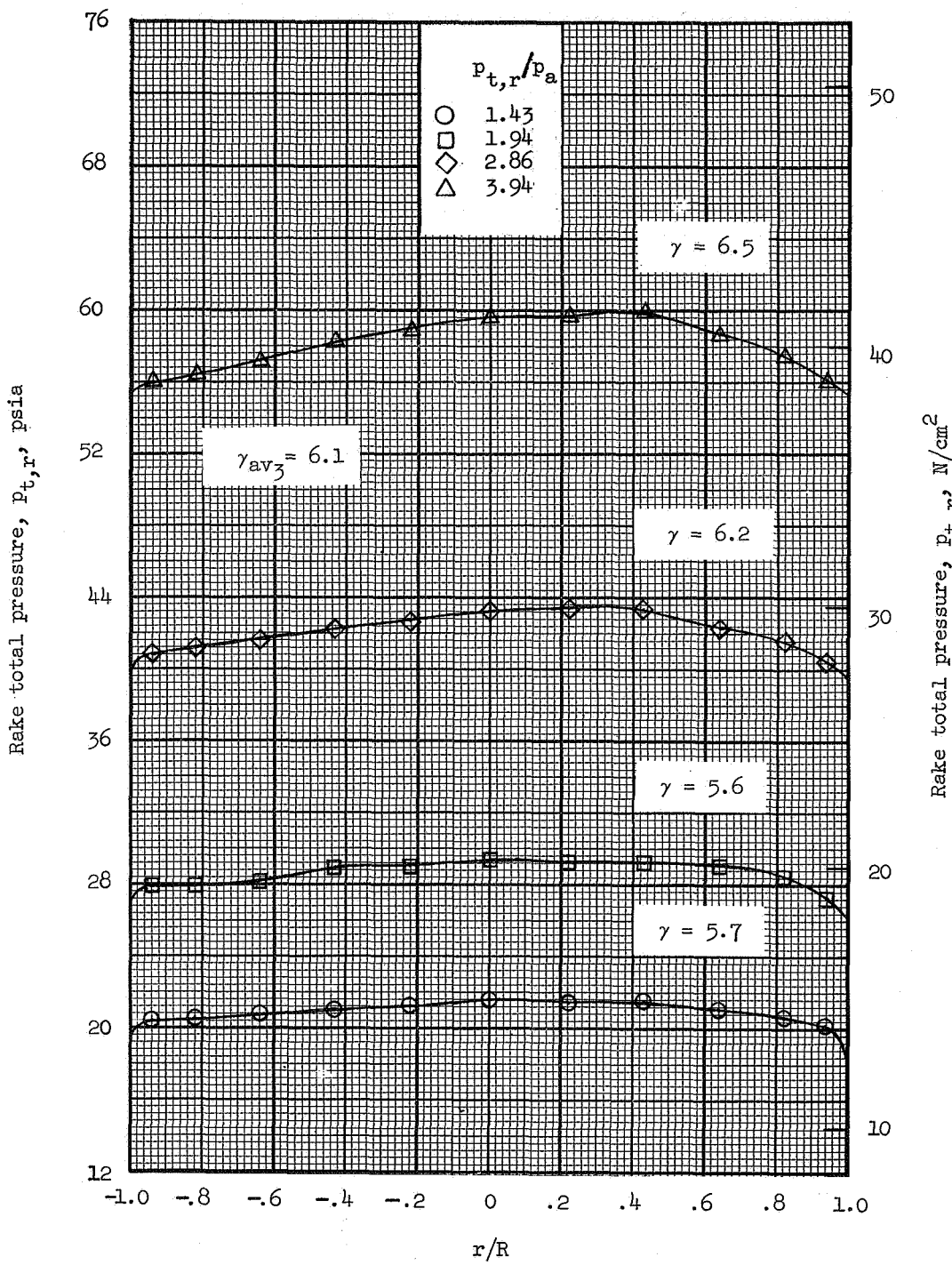

(f) Configuration IIIC. Engine 2.

Figure 8.- Continued.

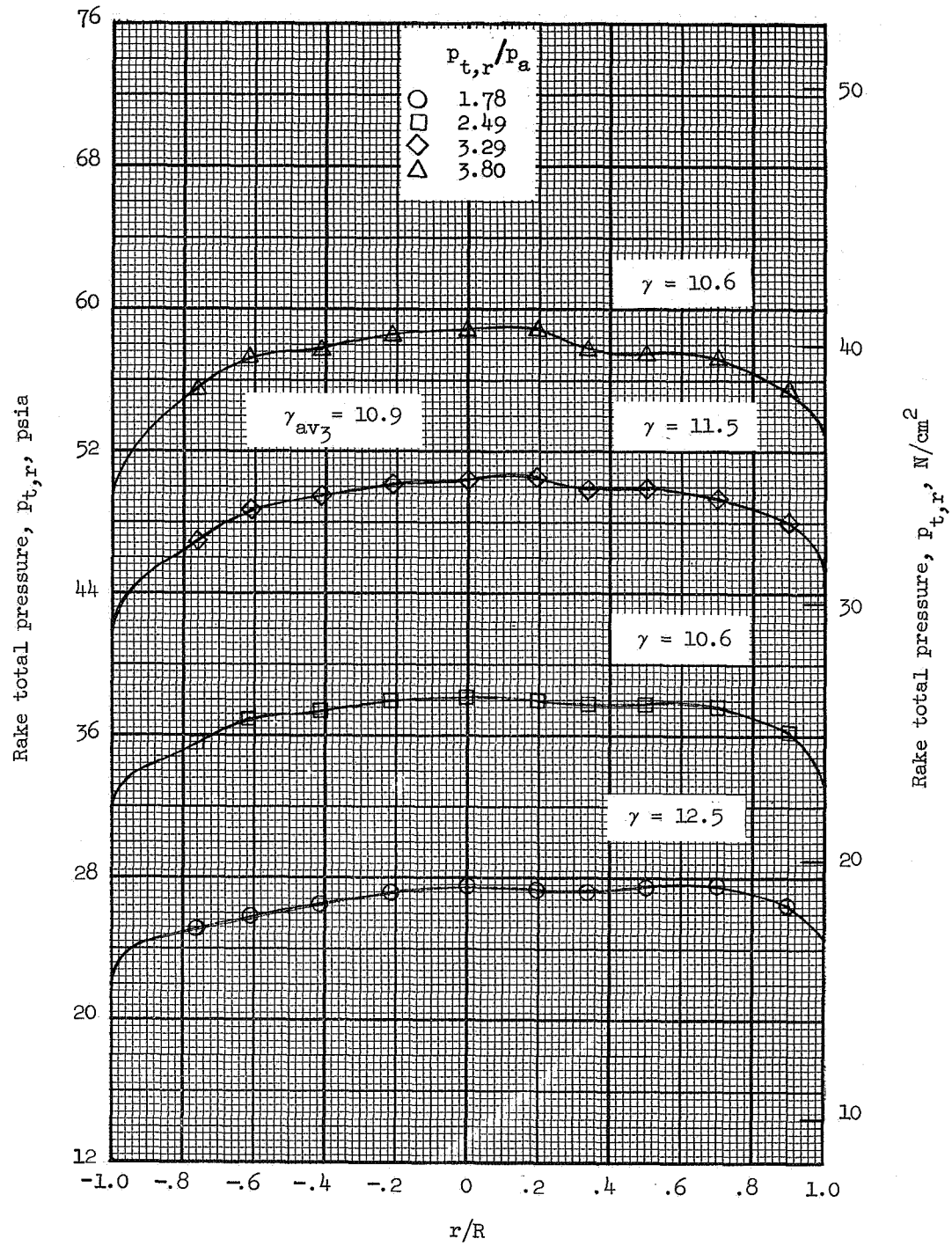

(g) Configuration IIIC, after 2.55 hours running time. Engine 3.

Figure 8.- Continued.

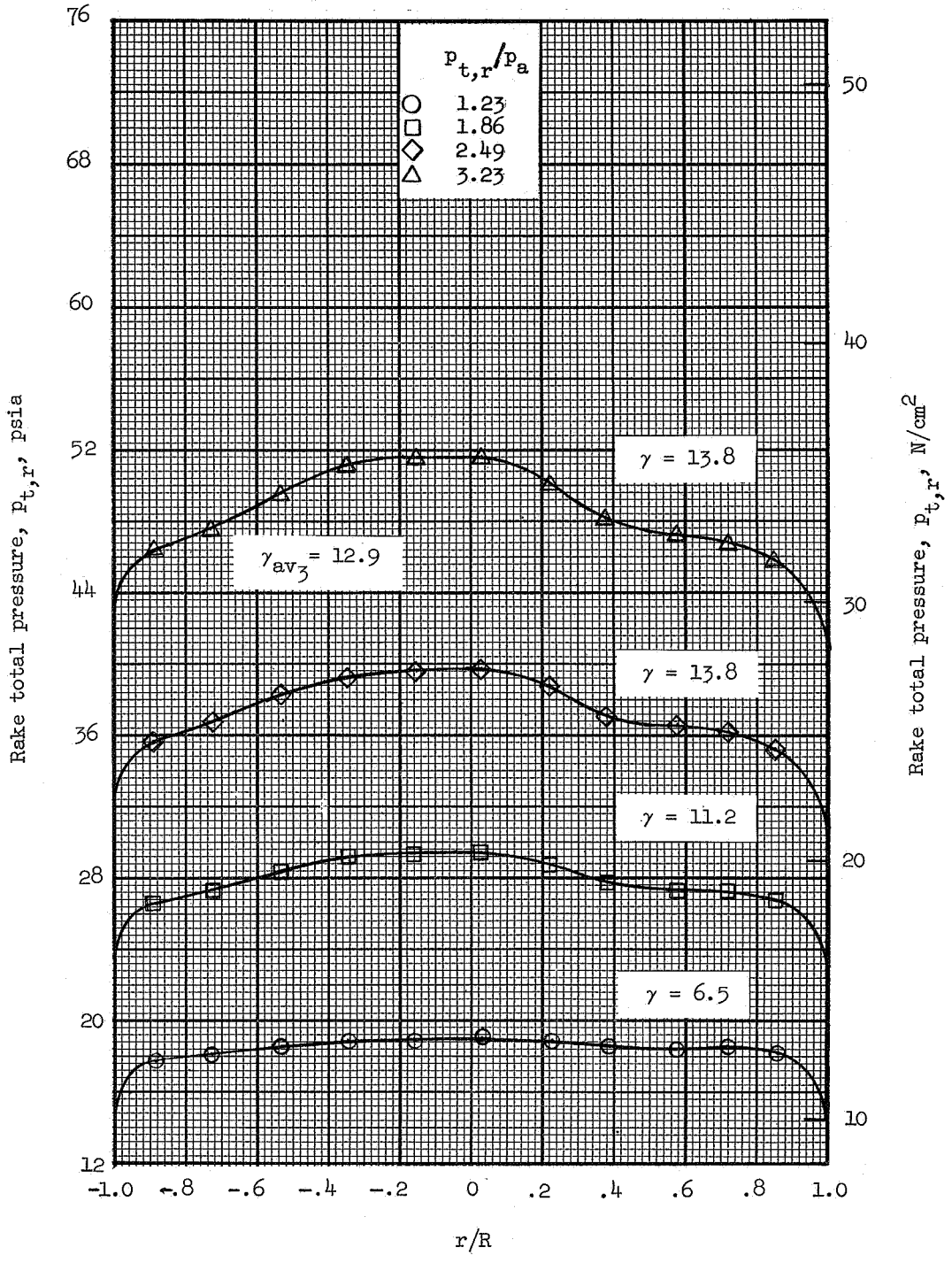

(h) Configuration IIID.

Figure 8.- Continued.

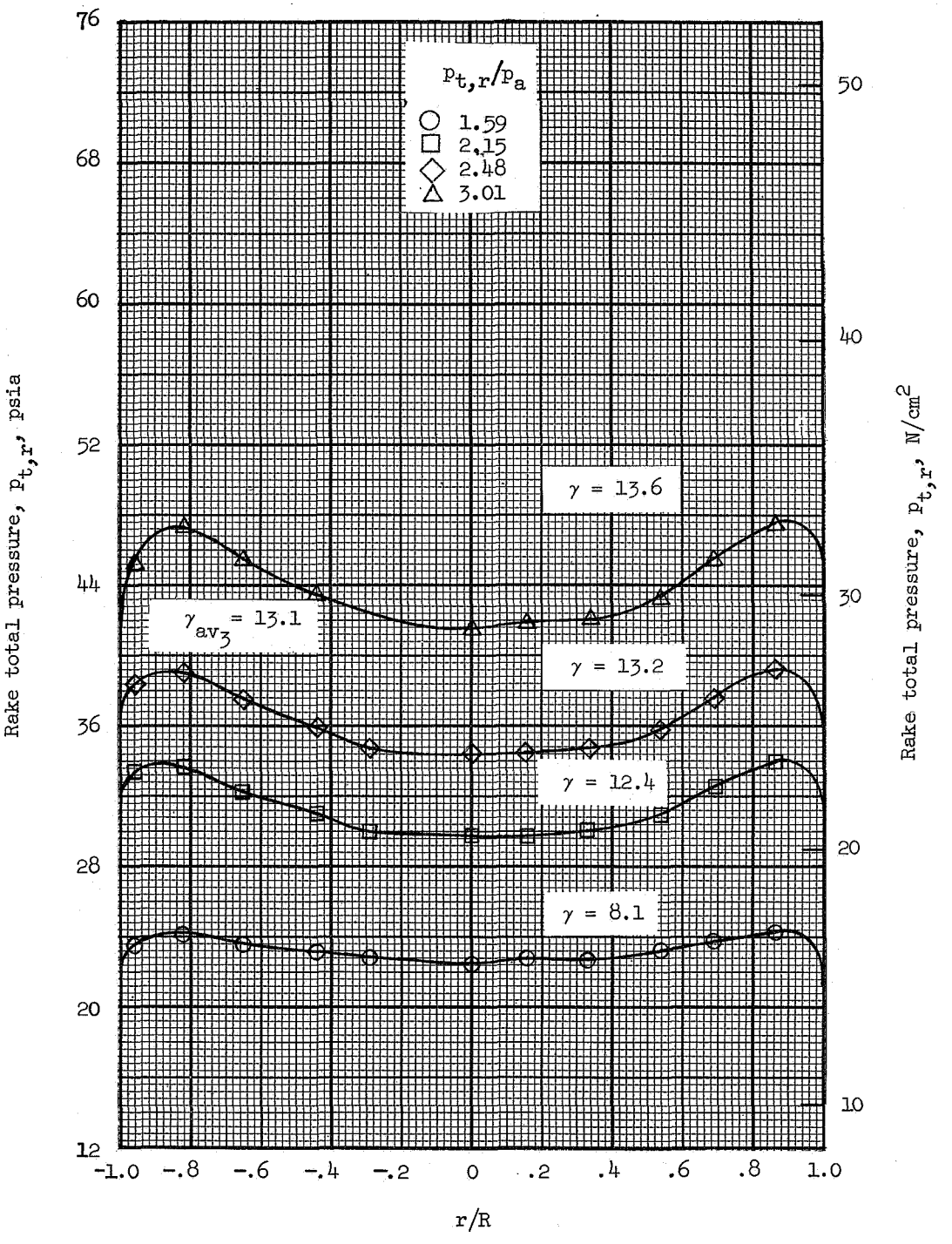

(i) Configuration IV.

Figure 8.- Continued.

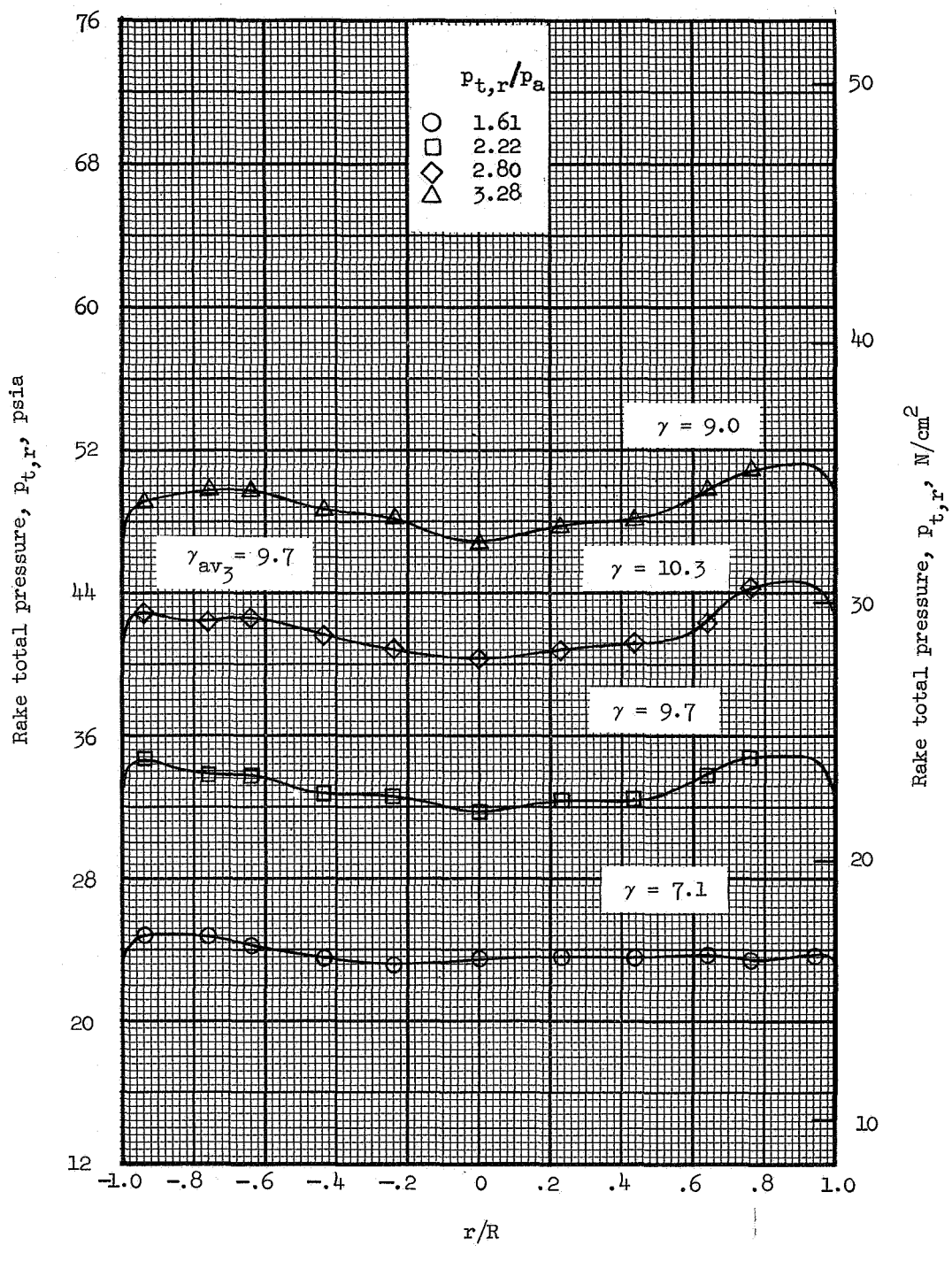

(j) Configuration V.

Figure 8.- Continued.

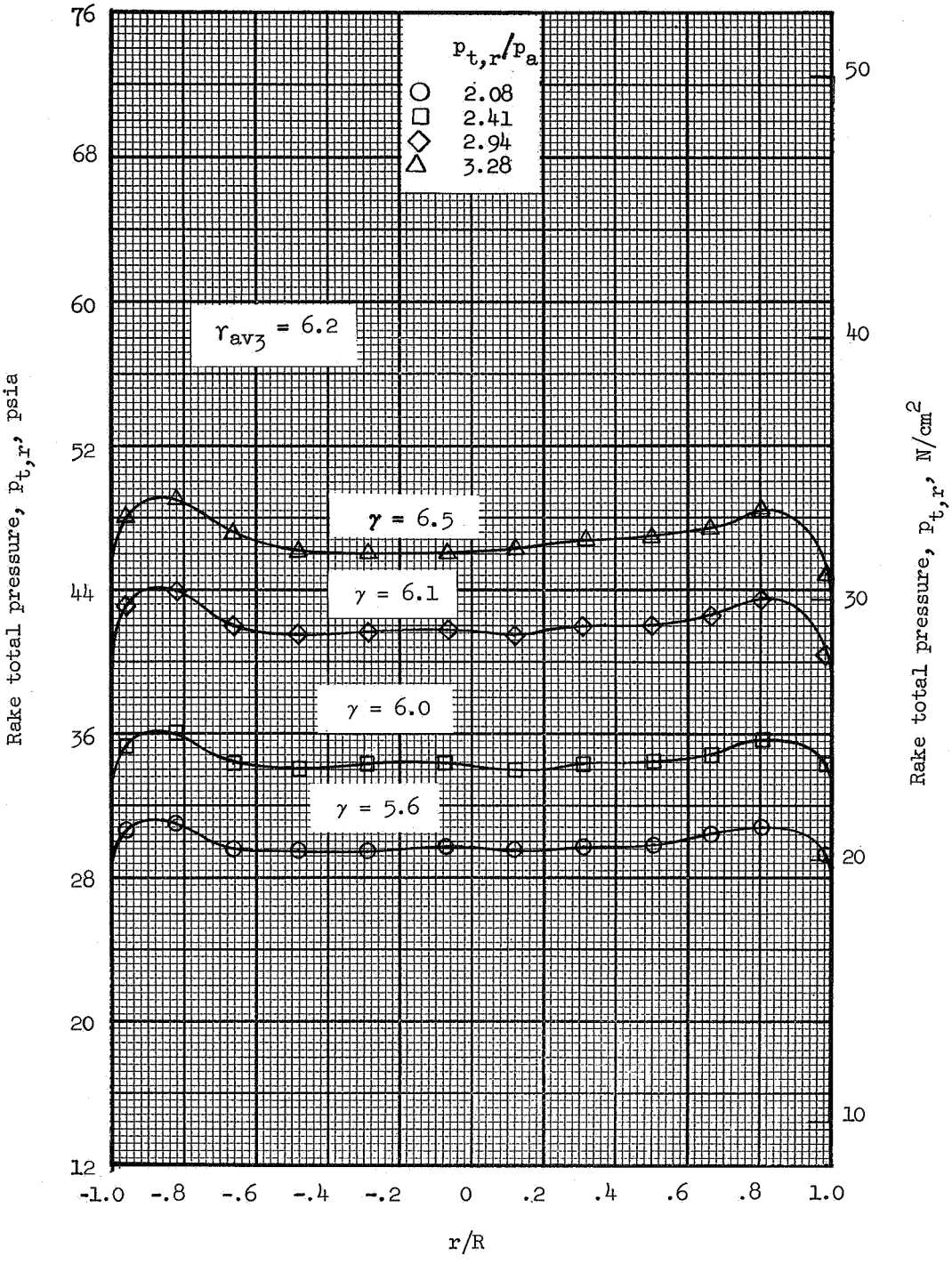

(k) Configuration VI.

Figure 8.- Continued.

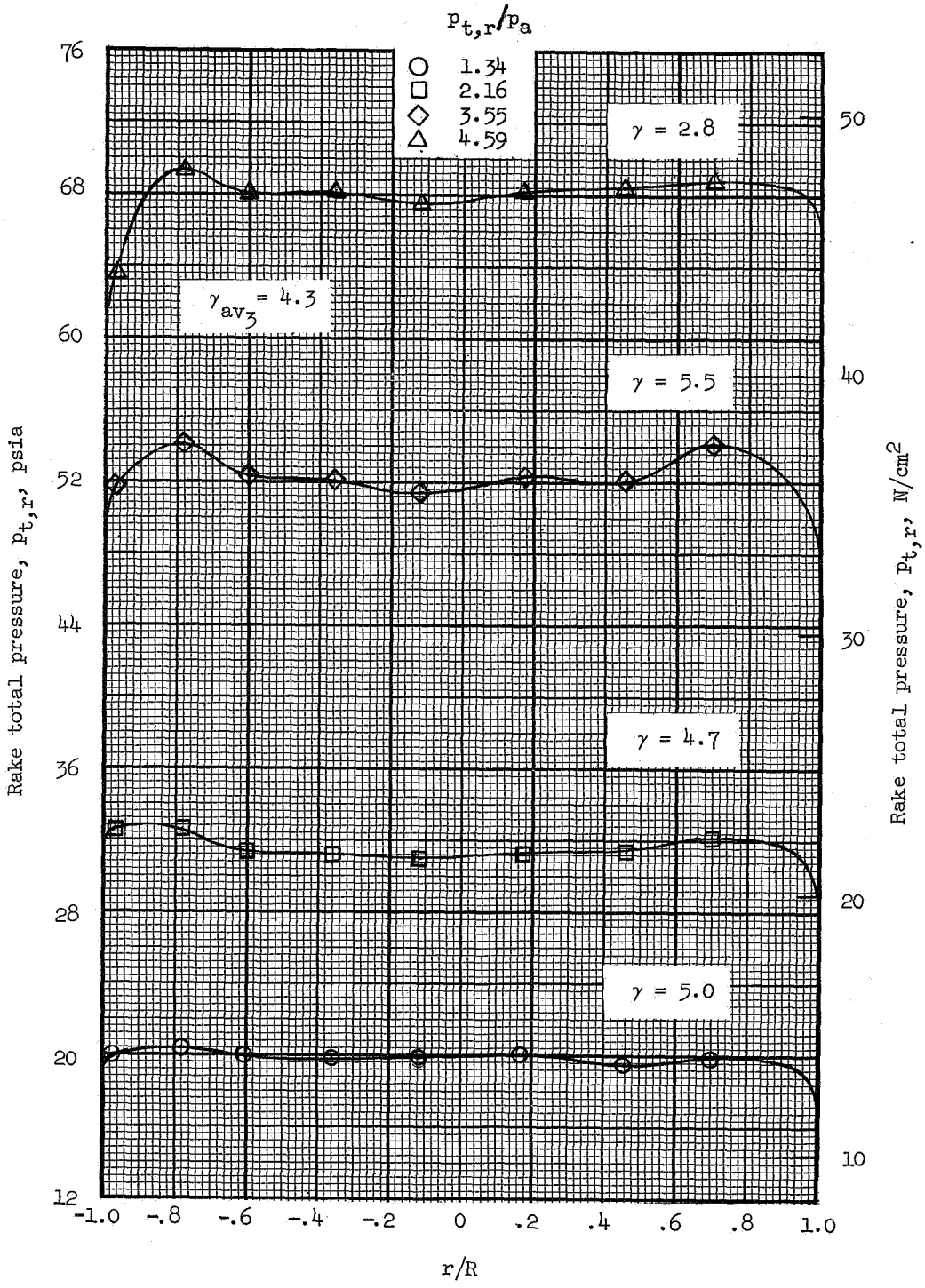

(l) Configuration VII.

Figure 8.- Continued.

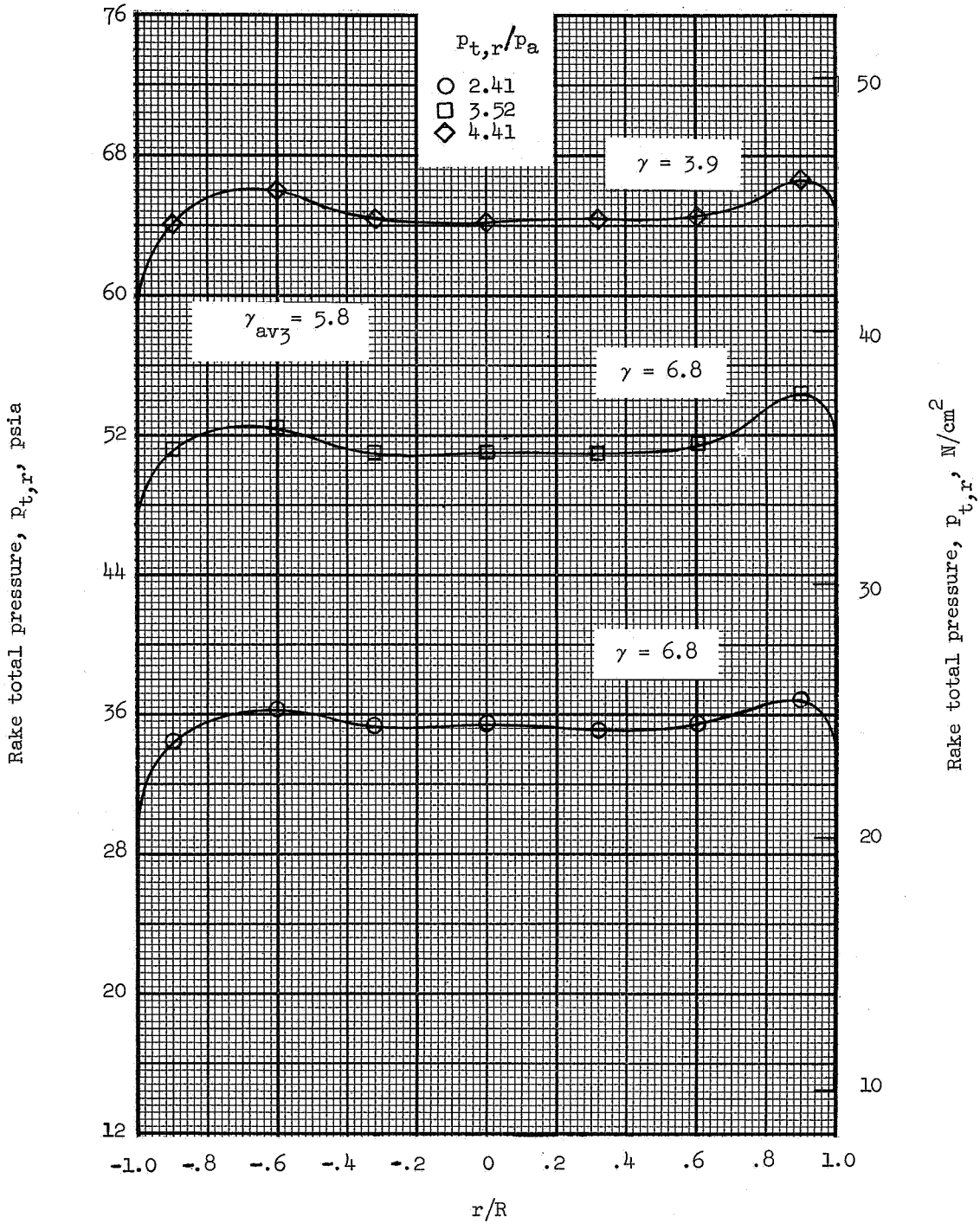

(m) Configuration VIII.

Figure 8.- Continued.

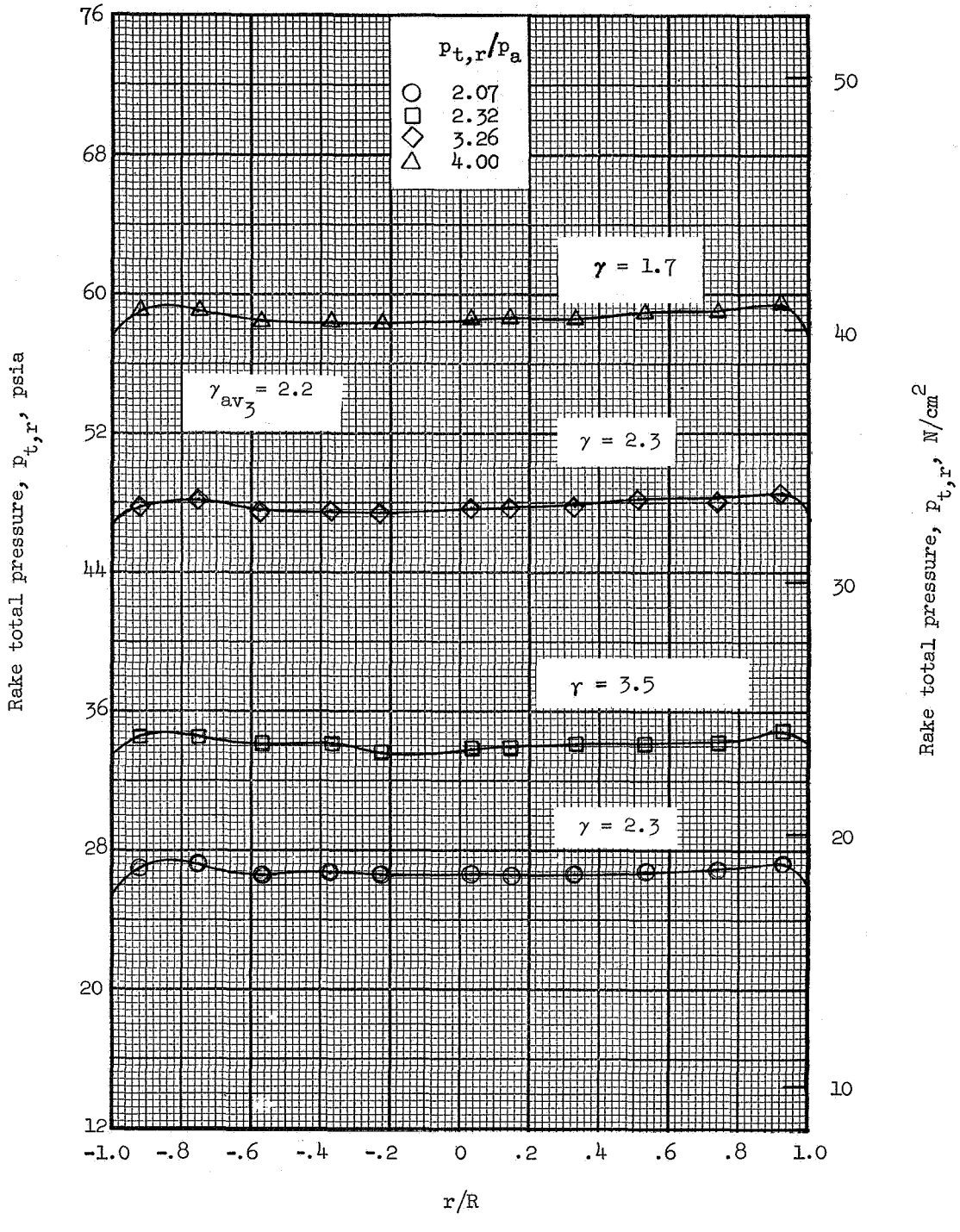

(n) Configuration IX.

Figure 8.- Concluded.

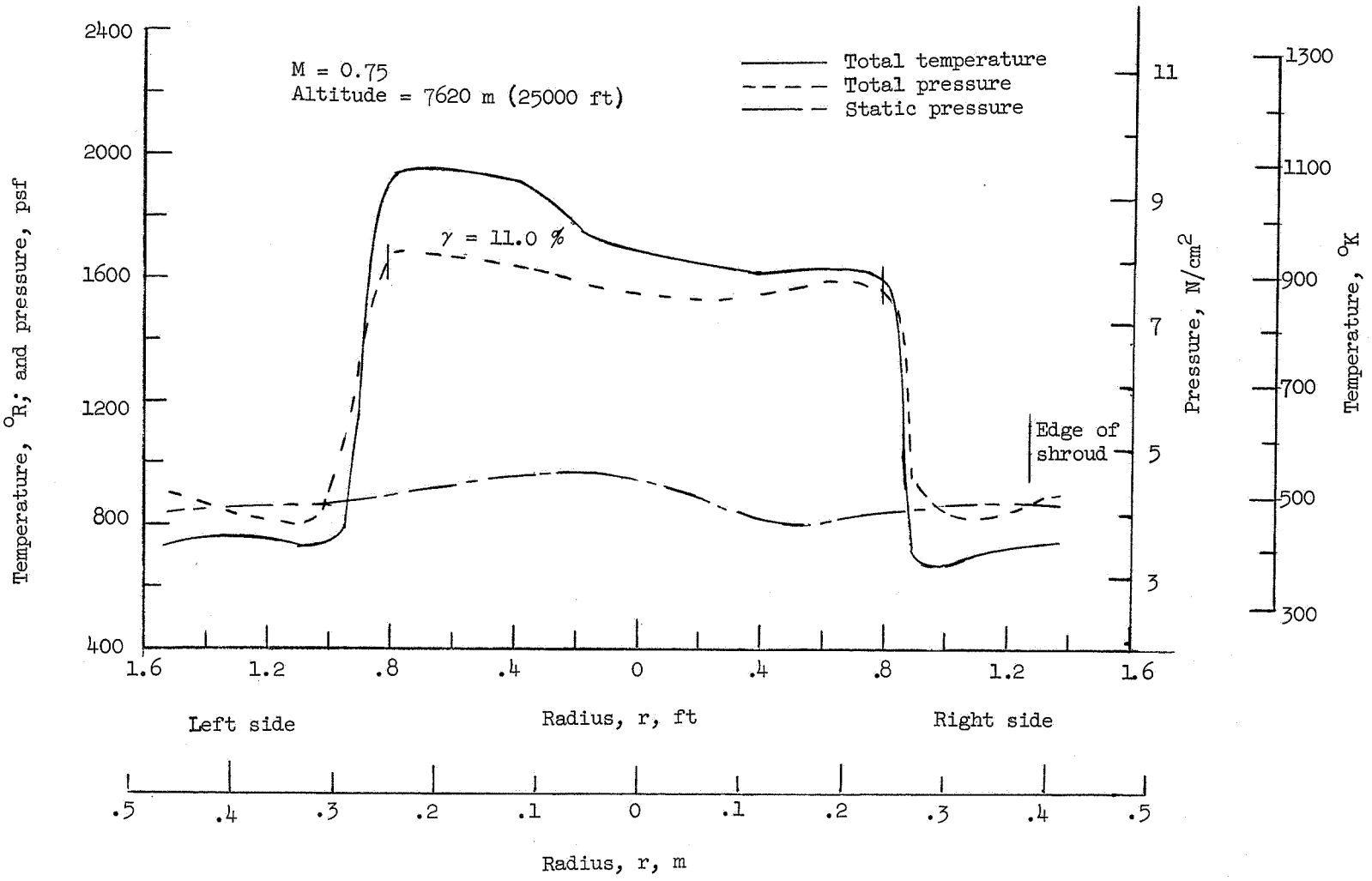

Figure 9.- Typical pressure and temperature distributions for J48-P8 engine with afterburner off. (From ref. 3.)

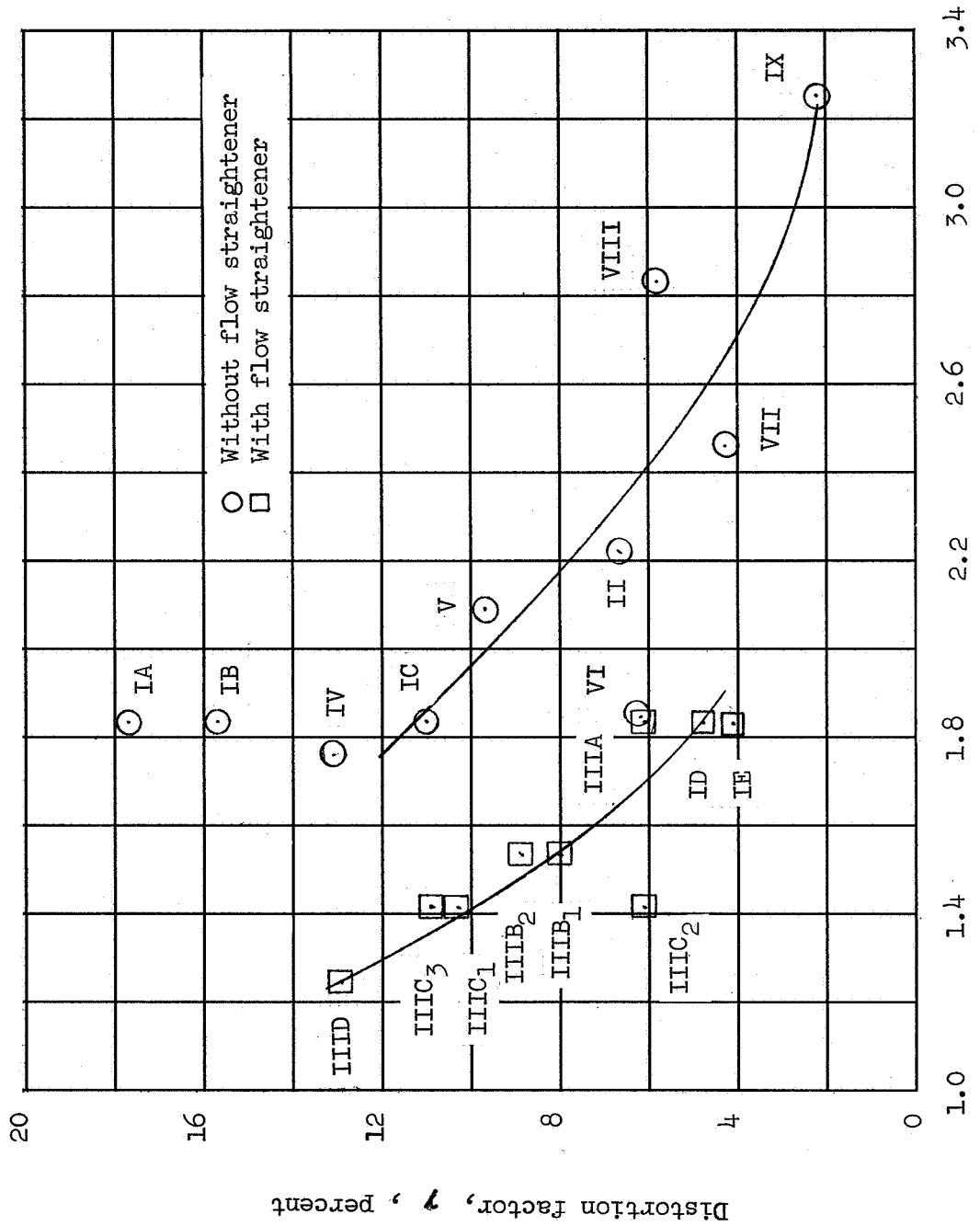

Figure 10.- Variation of distortion factor with engine tailpipe contraction ratio for various configurations.

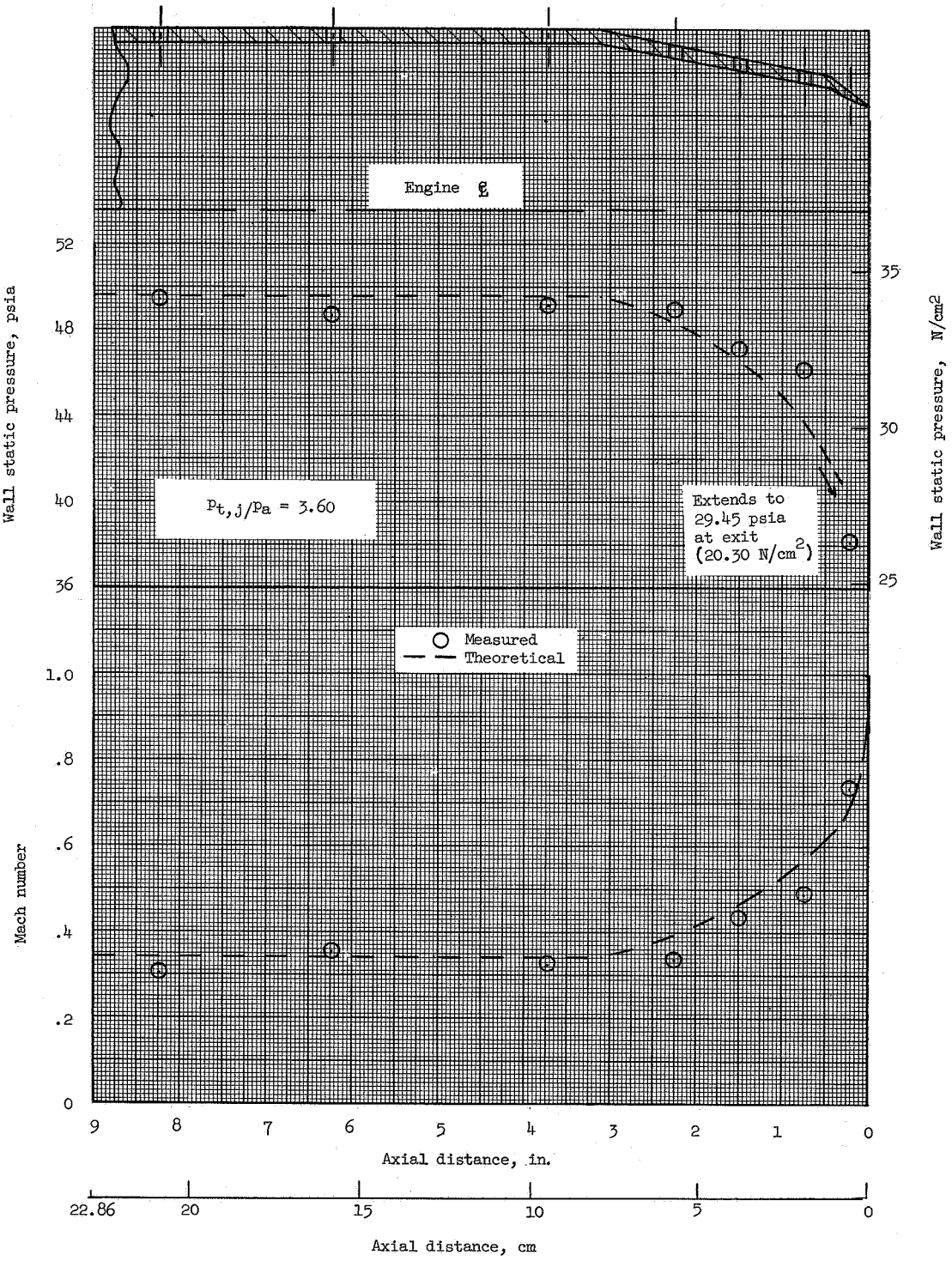

Figure 11.- Comparison of measured wall static-pressure distribution with theoretical and of calculated Mach number distribution with theoretical. Configuration 1B.

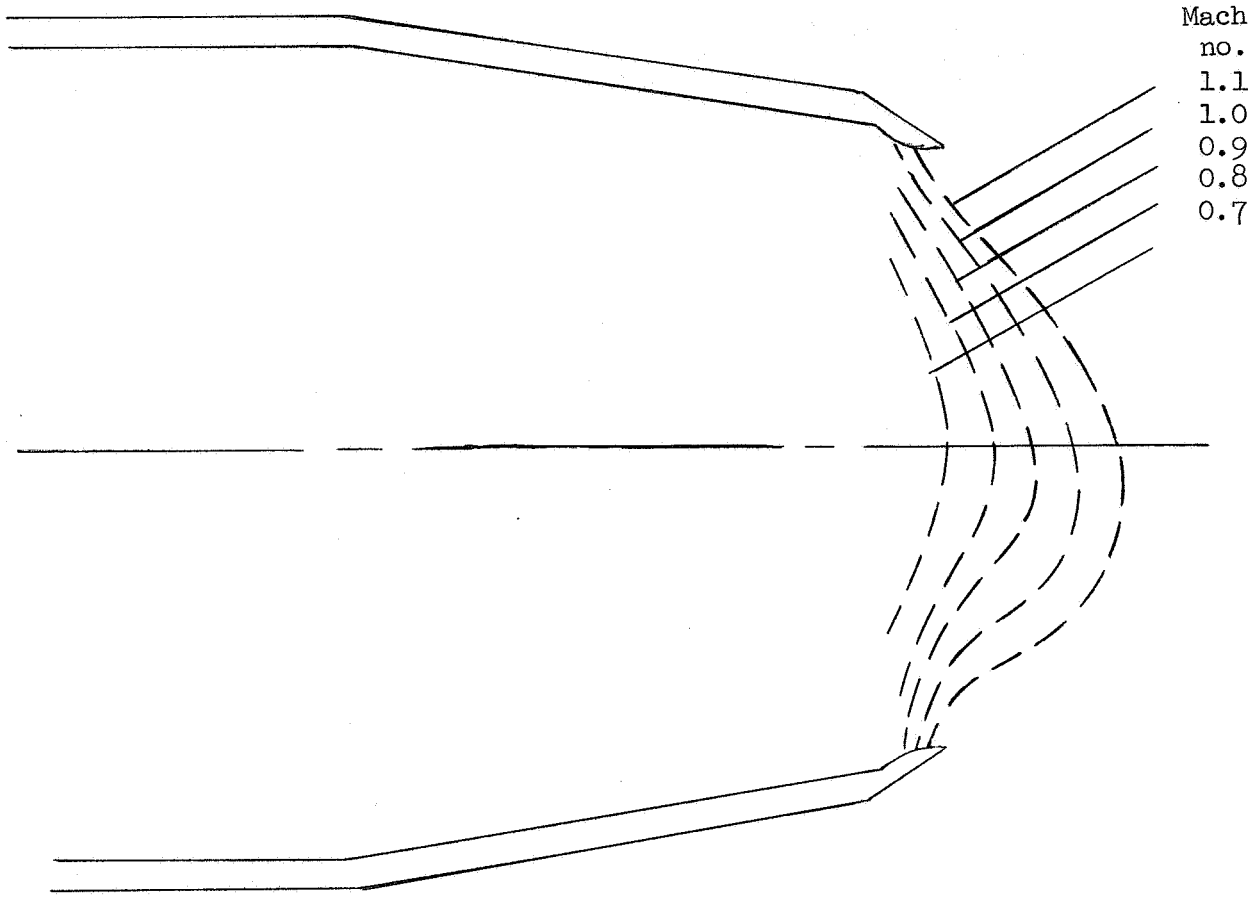

(a) Lines of constant Mach number. $p_{t,j}/p_a = 2.3$.

Figure 12.- Conditions near jet exit. Configuration 1B.

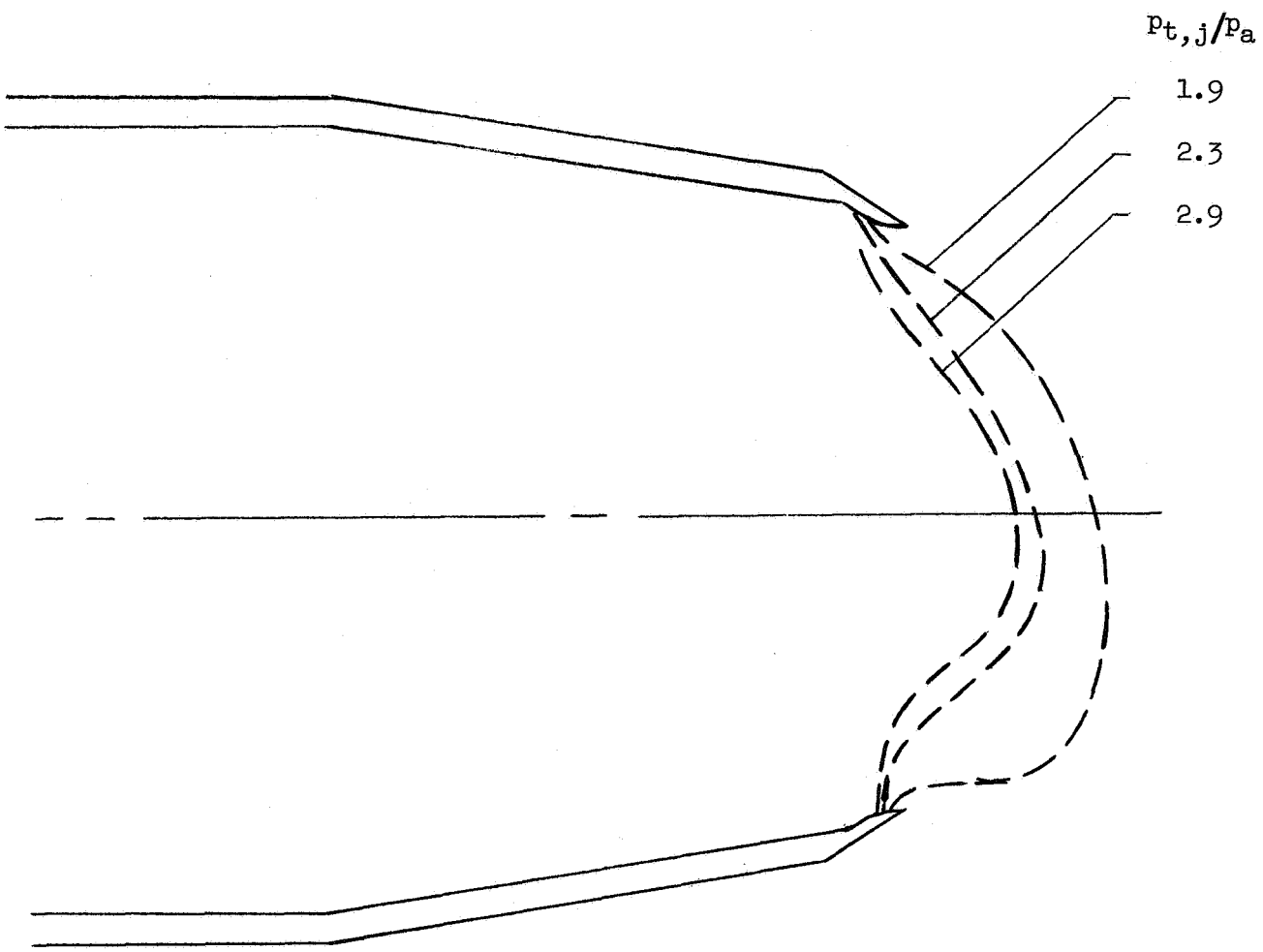

(b) Sonic lines at various pressure ratios.

Figure 12.- Concluded.

NATIONAL AERONAUTICS AND SPACE ADMINISTRATION
WASHINGTON, D.C. 20546

OFFICIAL BUSINESS

FIRST CLASS MAIL

POSTAGE AND FEES PAID
NATIONAL AERONAUTICS AND
SPACE ADMINISTRATION

POSTMASTER: If Undeliverable (Section 158
Postal Manual) Do Not Return

"The aeronautical and space activities of the United States shall be conducted so as to contribute . . . to the expansion of human knowledge of phenomena in the atmosphere and space. The Administration shall provide for the widest practicable and appropriate dissemination of information concerning its activities and the results thereof."

— NATIONAL AERONAUTICS AND SPACE ACT OF 1958

NASA SCIENTIFIC AND TECHNICAL PUBLICATIONS

TECHNICAL REPORTS: Scientific and technical information considered important, complete, and a lasting contribution to existing knowledge.

TECHNICAL NOTES: Information less broad in scope but nevertheless of importance as a contribution to existing knowledge.

TECHNICAL MEMORANDUMS: Information receiving limited distribution because of preliminary data, security classification, or other reasons.

CONTRACTOR REPORTS: Scientific and technical information generated under a NASA contract or grant and considered an important contribution to existing knowledge.

TECHNICAL TRANSLATIONS: Information published in a foreign language considered to merit NASA distribution in English.

SPECIAL PUBLICATIONS: Information derived from or of value to NASA activities. Publications include conference proceedings, monographs, data compilations, handbooks, sourcebooks, and special bibliographies.

TECHNOLOGY UTILIZATION PUBLICATIONS: Information on technology used by NASA that may be of particular interest in commercial and other non-aerospace applications. Publications include Tech Briefs, Technology Utilization Reports and Notes, and Technology Surveys.

Details on the availability of these publications may be obtained from:

SCIENTIFIC AND TECHNICAL INFORMATION DIVISION

NATIONAL AERONAUTICS AND SPACE ADMINISTRATION

Washington, D.C. 20546